Statistical Error Decomposition of Regional-Scale Climatological Precipitation Estimates from the Tropical Rainfall Measuring Mission (TRMM)

BRAD L. FISHER

Laboratory for Atmospheres and Science Systems and Applications, NASA Goddard Space Flight Center, Greenbelt, Maryland

(Manuscript received 7 February 2006, in final form 25 September 2006)

ABSTRACT

Monthly rainfall estimates inferred from the NASA Tropical Rainfall Measuring Mission (TRMM) satellite contain errors due to discrete temporal sampling and remote spaceborne rain retrievals. This paper develops a regional-scale error model that uses the rain information in the ground data to disentangle the sampling and retrieval errors in the satellite estimate statistically. The proposed method computes a mean rain rate from monthly rainfall statistics for each TRMM rain sensor by subsampling high-resolution ground-based rain data at satellite overpass times. This additional rain-subsampled parameter plays an essential role in the statistical decomposition of the total error distribution into its sampling and retrieval error components. Using the statistical formalism developed in this study, an error analysis was performed on 5 yr of monthly rain estimates produced by the TRMM Microwave Imager (TMI) and precipitation radar (PR) rain sensors aboard TRMM over a quasi $2° \times 2°$ region of the TRMM ground validation (GV) site at Melbourne, Florida. Annual retrieval and sampling error statistics were computed for the TMI and PR using monthly rainfall estimates derived from two independent ground-based sensors: a regional rain gauge network and the Next-Generation Weather Radar (NEXRAD). Subsampled ground-based rainfall estimates produced for the radar and the gauges were highly correlated with the TMI and PR rainfall estimates, and both GV sensors produced relatively consistent error estimates. The PR-to-TMI sampling error ratio was equal to about 1.3, which was in close agreement with prelaunch predications, and the TMI-to-PR retrieval error ratio was about 2.0. For the TMI, a seasonally alternating rainfall bias was also observed that was negative during winter and positive during summer.

1. Introduction

The Tropical Rainfall Measuring Mission (TRMM) satellite collects rainfall information from a low earth orbit from a dual complement of passive and active rain sensors (Kummerow et al. 1998). Climate modelers, hydrologists, and forecasters use TRMM rain products to investigate a broad range of scientific questions on the earth's hydrological cycle, including the role of clouds and precipitation in forcing climate change. TRMM rain estimates, however, incur sampling and retrieval errors that affect the accuracy of the satellite-inferred rain information provided to users. An important goal of the TRMM Ground Validation Program has subsequently been to determine the random and systematic errors associated with TRMM rainfall estimates on monthly climate scales over areas approximating 10^5 km^2 (Simpson et al. 1988).

Prior to the launch of TRMM, Wilheit (1988) proposed an error model for TRMM that related the total error in climatological precipitation estimates to contributions from sampling, random instrument errors, and correlated algorithm-related errors. Wilheit discerned that the bulk of the TRMM error budget would consist mainly of temporal sampling errors, associated with the process of discrete temporal sampling, and correlated retrieval errors. Although sampling and retrieval errors are incurred independently, they become entangled in the statistical integrations of monthly rainfall produced from instantaneous TRMM snapshots.

The error structure quantitatively determines how much a satellite rain estimate deviates from its true value. However, the true mean rainfall (i.e., perfect measurement with zero error) is an ideal parameter that is never measured directly, given that all empirical observations of surface rainfall contain intrinsic mea-

Corresponding author address: Brad L. Fisher, NASA/GSFC, Code 912.1, Greenbelt, MD 20771.
E-mail: fisher@radar.gsfc.nasa.gov

DOI: 10.1175/JAM2497.1

© 2007 American Meteorological Society

surement/estimation errors. Empirical satellite validation often involves statistical comparisons of the satellite rain estimates with high-quality surface rain data from ground sensors (Thiele 1988), where the error structure is quantitatively better understood, therefore providing a more reliable linkage between the satellite estimate and the true rainfall.

The utilization of surface-based sensors to validate satellite-inferred rain estimates can introduce a host of other error sources that will tend to broaden the statistical error distribution. Any satellite validation strategy has to consider the following: the natural variability of precipitation over a broad range of spatiotemporal scales (i.e., the autocorrelation function); the disproportionate distribution of rain measurements over land versus the oceans, where oceans cover three-quarters of the earth's surface (i.e., geohistoric sampling bias); continuous versus discrete sampling scenarios; and satellite algorithm uncertainties and other measurement uncertainties such as noncontiguous spatial sampling of rain gauges, systematic gauge errors related to instrumentation and site location, imperfect reflectivity–rain rate (Z–R) relations, and radar beam filling.

As the TRMM satellite orbits the earth, its rain sensors sample the regional atmosphere only at discrete time intervals. Monthly estimates of rainfall are then statistically generated from the unconditional sampling statistics for each month (North 1992), defined as the mean monthly rain rate computed from all the observations collected in a month at some regional scale (minimum resolution is about 0.5°). Sampling the atmosphere at discrete time intervals, though, produces an intrinsic sampling error that depends on the orbital frequency, the autocorrelation time (a climatological parameter), the natural variability of rainfall (i.e., standard deviation), and the area covered by the satellite footprint (Laughlin 1981; Shin and North 1988; Steiner et al. 2003; Gebremichael and Krajewski 2004). Variations in the orbital frequency and climatological conditions can also contribute to the sampling error variance considered over time scales longer than 1 month (Fisher 2004).

The effects of temporal sampling errors on satellite rain estimates were studied extensively during the prelaunch phase of the TRMM mission. Laughlin (1981), Shin and North (1988), North and Nakamoto (1989), and Bell et al. (1990), using statistically based parametric models, predicted random sampling errors ranging from 8% to 12% per month relative to the mean rainfall. Other empirical studies by McConnell and North (1987), Oki and Sumi (1994), and Steiner (1996) estimated sampling errors by subsampling ground data at periodic intervals and reported results consistent with theoretical methods.

Sampling errors introduce a kind of statistical noise into the monthly rain estimate that broadens the error distribution, further complicating the task of evaluating the retrieval errors associated with the rain algorithms. TRMM retrieval errors tend to be linked to the physics of the rain algorithms and are of particular interest because they can be corrected either through a bias adjustment or subsequent improvements to the rain algorithms. It is therefore important to understand the error characteristics of the TRMM rain algorithms for different climatological regions to evaluate the data quality and to provide constructive feedback to algorithm developers.

This paper develops an error model for determining the sampling and retrieval errors for the TRMM Microwave Imager (TMI) and the precipitation radar (PR) over a TRMM satellite validation site in Melbourne, Florida. The model generates additional statistical degrees of freedom by computing secondary subsampled rain estimates from two validation datasets, consisting of 5 yr of radar and gauge data (1998–2002), which is applied to the gridded region shown in Fig. 1, covering a contiguous region defined by ten 0.5° grid boxes that fall inside the 2° × 2° gridded region shown in the figure.

This paper has been subdivided into seven sections. Section 2 describes the theoretical method involved in the decomposition of sampling and retrieval errors from the total error budget. Section 3 describes the data products used in this study, including descriptions of the satellite and ground instrumentation. Section 4 analyzes the rainfall climatology of central Florida as determined from the various rain parameters generated from the 5 yr of data. Section 5 examines the radar–gauge correlations and error structures, and section 6 applies the error model developed in section 2 to regional TMI and PR rainfall estimates and analyzes the results. A summary and discussion of the results and method are provided in section 7.

2. Error distribution statistics

In this section, we will develop a statistical error model for disentangling the sampling and retrieval errors in TRMM rainfall estimates. The errors in both satellite and ground rain estimates are ideally evaluated relative to the true time–area-averaged rain rate r_T. For an arbitrary grid box of area A on the earth's surface and integration time T (~1 month), r_T is defined as

$$r_T = \frac{1}{T}\int_0^T dt \frac{1}{A}\int_A r(x, t)\, d^2x, \tag{1}$$

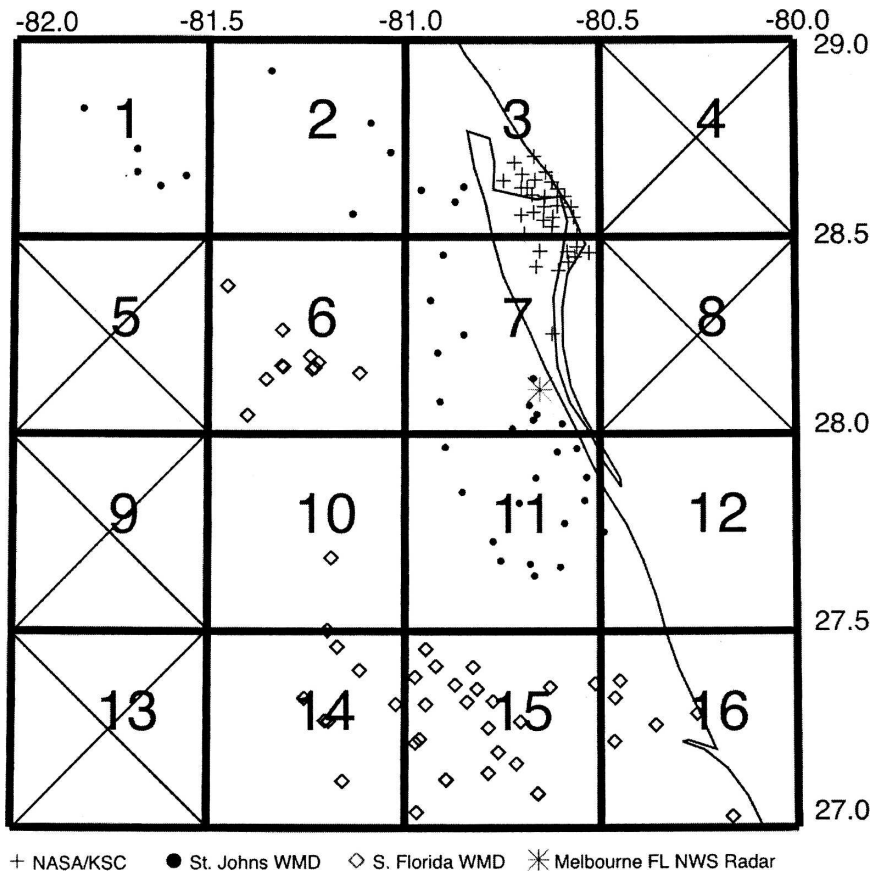

FIG. 1. Regional map of central Florida showing 2° × 2° gridded region partitioned into 0.5° grid boxes. The map illustrates the overall distribution of rain gauges consisting of three different gauge networks: KSC (plus signs), STJWMD (filled circles), and SFWMD (diamonds). Grid boxes not containing gauges are designated with an X. These boxes were not used in the error analysis.

where $r(x, t)$ is the true instantaneous surface rain rate at a point in the continuous domain of A. It is assumed that r_T does not depend on the observational frame of reference (i.e., spaceborne and ground-based reference frames are considered to be equivalent with respect to r_T).

Each time the TRMM satellite flies over A, it collects instantaneous rain-rate information s_i. However, the field of view (FOV) of the TRMM sensors will not always cover the entire area represented by A but rather will sample a subregion A_i of A, where $A_i \leq A$ (Bell and Kundu 2000). The satellite-estimated time–area-averaged rain rate s_0 can then be computed as the sum of all the observations, including a weighting factor that accounts for the partial coverage of the satellite

$$s_0 = \frac{1}{n}\sum_{i=1}^{n} \omega_i s_i, \tag{2}$$

where $\omega_i \propto A_i/A$ and n is the number of observations collected by the satellite during a 1-month period. Note that ω_i is normalized such that

$$n^{-1}\sum_{i=1}^{n} \omega_i = 1.$$

The separation of the total error variance into sampling and retrieval components will now be derived using the conceptual approach developed by Bell and Kundu (2000) and Bell et al. (2001). In this error model, we consider a hypothetical geosynchronous TRMM-like satellite that continuously samples the whole area associated with A using passive and active remote sensors identical to the TMI and PR. The rain estimate inferred from this hypothetical situation is defined as s_G. Estimate s_G is assumed to have the same measurement accuracy as s_0, but since it measures A continuously, s_G will not incur any temporal sampling errors.

Because s_G does not incur sampling errors, it is distinguished from s_0, which contains both sampling and retrieval errors.

Using the definitions of s_G, s_0, and r_T, the true temporal sampling and retrieval errors associated with the TRMM rain estimate s_0 for a single month can be defined as

$$\varepsilon_{\mathrm{Tsam}} = s_0 - s_G \quad \text{and} \tag{3}$$

$$\varepsilon_{\mathrm{Tret}} = s_G - r_T\,. \tag{4}$$

The definitions in (3) and (4) can then be used to derive a general expression for the error variance, defined as

$$\begin{aligned}\mathrm{var}(s_0 - r_T) &= \mathrm{var}(\varepsilon_{\mathrm{Tsam}} + \varepsilon_{\mathrm{Tret}}) \\ &= \mathrm{var}(\varepsilon_{\mathrm{Tsam}}) + \mathrm{var}(\varepsilon_{\mathrm{Tret}}) \\ &\quad + 2\,\mathrm{cov}(\varepsilon_{\mathrm{Tsam}}, \varepsilon_{\mathrm{Tret}}).\end{aligned} \tag{5}$$

It is now assumed that the sampling and retrieval errors are uncorrelated [i.e., $\mathrm{cov}(\varepsilon_{\mathrm{Tsam}}, \varepsilon_{\mathrm{Tret}}) \approx 0$]. This is to say that if the samples collected over A are statistically independent, then the error in the physical measurement should not generally depend on when and where the measurement was taken. This assumption results in the following simplification of (5):

$$\mathrm{var}(s_0 - r_T) \approx \mathrm{var}(\varepsilon_{\mathrm{Tsam}}) + \mathrm{var}(\varepsilon_{\mathrm{Tret}}) = \sigma^2_{\mathrm{Tsam}} + \sigma^2_{\mathrm{Tret}}, \tag{6}$$

where σ^2_{Tsam} and σ^2_{Tret} are distinguished as the true sampling and retrieval error variances with respect to r_T.

In most validation studies, an empirical reference r_0, such as the monthly rainfall estimate inferred from an areal network of rain gauges, is used in place of r_T. The empirical reference r_0 introduces an additional error variance σ^2_{val} that accounts for random, systematic, and sampling errors in the ground-based validation products (Bell and Kundu 2003; Fisher 2004).

Using r_0, we can then rewrite the argument appearing on left side of (6) as

$$\mathrm{var}(s_0 - r_T) = \mathrm{var}[(s_0 - r_0) + (r_0 - r_T)]. \tag{7}$$

If we assume that the terms $(s_0 - r_0)$ and $(r_0 - r_T)$ in (7) are uncorrelated, we can then use (6) and (7) to approximate the true error variance as

$$\begin{aligned}\mathrm{var}(s_0 - r_T) &\approx \mathrm{var}(s_0 - r_0) + \mathrm{var}(r_0 - r_T) \\ &\approx \sigma^2_{\mathrm{sam}} + \sigma^2_{\mathrm{ret}} + \sigma^2_{\mathrm{val}}.\end{aligned} \tag{8}$$

Note that σ^2_{sam} and σ^2_{ret} in (8) now characterize the relative sampling and retrieval error variances (i.e., s_0 is considered relative to r_0 instead of r_T). We also assume that the bulk of the error associated with the validation sensor estimate is characterized by $\mathrm{var}(r_0 - r_T)$ [i.e., $\sigma^2_{\mathrm{val}} \approx \mathrm{var}(r_0 - r_T)$].

The validation reference r_0 does not by itself provide enough information to disentangle the sampling and retrieval errors associated with each independent error distribution. However, if the time resolution of the ground-based data is sufficiently high that the time series can be sampled at satellite overpass times, then a subsampled rainfall estimate r_S can be computed that incorporates the temporal sampling statistics of a particular TRMM rain sensor into the ground-based rain estimate. Because the ground-based rainfall time series is only subsampled during TRMM overpasses, it is assumed that r_S and s_0 incur equivalent temporal sampling errors.

The subsampled parameter r_S performs a critical role in the decomposition of $\mathrm{var}(s_0 - r_0)$ into sampling and retrieval error components, similar to the role of s_G in the derivation of (3), (4), and (5). Note, however, that, while s_G does not contain any temporal sampling errors (the hypothetical satellite collects data continuously over A), r_S does include the temporal sampling error of the satellite (r_S is subsampled from the quasi-continuous r_0 time series at satellite overpass times).

We first define the sampling and retrieval errors for a single measurement as

$$\varepsilon_{\mathrm{ret}} = s_0 - r_S \quad \text{and} \tag{9}$$

$$\varepsilon_{\mathrm{sam}} = r_S - r_0. \tag{10}$$

Equations (9) and (10) can then be inserted into the argument of $\mathrm{var}(s_0 - r_0)$, and, assuming as before that sampling and retrieval errors are uncorrelated, we obtain the following approximation for the error variance relative to empirical reference:

$$\mathrm{var}(s_0 - r_0) \approx \mathrm{var}(\varepsilon_{\mathrm{sam}}) + \mathrm{var}(\varepsilon_{\mathrm{ret}}) = \sigma^2_{\mathrm{sam}} + \sigma^2_{\mathrm{ret}}. \tag{11}$$

The relative sampling and retrieval errors are then approximated from (8) and (11) as

$$\sigma^2_{\mathrm{sam}} \approx \mathrm{var}(\varepsilon_{\mathrm{sam}}) = \sigma^2_{r_S} + \sigma^2_{r_0} - 2\,\mathrm{cov}(r_S, r_0) \quad \text{and} \tag{12}$$

$$\sigma^2_{\mathrm{ret}} \approx \mathrm{var}(\varepsilon_{\mathrm{ret}}) = \sigma^2_{s_0} + \sigma^2_{r_S} - 2\,\mathrm{cov}(s_0, r_S), \tag{13}$$

where $\sigma^2_{s_0}$, $\sigma^2_{r_S}$, and $\sigma^2_{r_0}$ are natural variances computed from s_0, r_S, and r_0, respectively.

This method for decomposing the satellite sampling and retrieval errors ensures a strong measure of statistical control, because the time series used to compute r_S represents a complete subset of the time series associated with r_0. Furthermore, because r_S and r_0 correspond

to real empirical observations, σ^2_{sam} in (12) accounts for variability in the sampling error due to climate-scale precipitation anomalies. However, σ^2_{sam} and σ^2_{ret} will not generally be equal to the σ^2_{Tsam} and σ^2_{Tret} because of the contribution of σ^2_{val}.

The bias is defined as the difference between the estimated quantity and the true quantity. In this validation model, relative sampling and retrieval biases, b_{sam} and b_{ret}, are estimated with respect to the empirical ground references as

$$b_{\mathrm{sam}} = \sum_{i=1}^{N} (r_S - r_0) \Big/ \sum_{i=1}^{N} r_0 \quad \text{and} \tag{14}$$

$$b_{\mathrm{ret}} = \sum_{i=1}^{N} (s_0 - r_S) \Big/ \sum_{i=1}^{N} r_S\,, \tag{15}$$

where N is the number of monthly data samples. Note that in both (14) and (15) the terms in the numerator and the terms in the denominator are summed independently. These two expressions treat the sampling and retrieval biases as a bulk climatological property of the error distribution.

3. Satellite and ground rain products and instrumentation

a. Satellite hardware and data products

1) TRMM RAIN SENSOR DESCRIPTIONS

The TRMM satellite was launched into a sun-asynchronous, low-earth orbit on 27 November 1997, with a sensor package that included two rain sensors (TMI and PR) designed to collect rainfall information over an annular region of the earth's surface between 40°S and 40°N. In August of 2001, the TRMM satellite underwent a boost from an average altitude of 350 km to an altitude of 402 km to conserve fuel and to extend the life of the mission. Global analysis of instantaneous TMI and PR rain rates have indicated that the boost only had a marginal affect on the TMI rain rates, but PR rain rates appear to have been lowered on average. Systematic changes in the PR rain rates due to the boost are still being investigated (J. Kwiatkowski 2006, personal communication).

The TMI is a passive rain sensor that has nine channels that sample terrestrial microwave radiation at five frequencies: 10.7, 19.4, 21.3, 37.0, and 85.5 GHz. Except for the 21.3-GHz channel, dual channels collect the horizontally (H) and vertically (V) polarized radiance information (only one V channel is reserved for 21.3 GHz). Whereas all nine channels are used in the determination of rain rates over oceanic regions of the earth's surface, TMI-derived rain rates over land are inferred from the rain information obtained from the two 85.5-GHz "scattering" channels because of ground contamination from the other channels that probe the precipitable water more directly (Spencer et al. 1989). Instantaneous TMI rain estimates are produced using the Goddard profiling algorithm developed by Kummerow et al. (1996). The algorithm has continued to evolve, and significant improvements to the algorithm are described in Kummerow et al. (2001).

The PR is the first spaceborne radar used in the collection of rain information and operates at a frequency of 13.8 GHz, with a horizontal resolution near nadir of about 4.3 km. The PR's superior vertical and horizontal resolution, however, is better suited for resolving smaller-scale precipitation features (Kummerow et al. 1998). Because the PR's sensitivity is only about 17 dBZ (~0.25 mm h^{-1}), some light rainfall goes undetected. In the low-level processing of the raw reflectivity data (i.e., level 1), a path attenuation correction is applied to correct for attenuation due to the intervening rain, because attenuation can be a significant source of error (Iguchi et al. 2000; Meneghini et al. 2000). The spatial sampling of the PR and TMI differ as a result of the different swath characteristics of each sensor. The swaths of the PR and TMI are 215 and 759 km, respectively. These differences in the areal coverage of the two sensors produce an expected sampling error for the PR that is about 1.3 times that of the TMI.

2) TMI AND PR MONTHLY ESTIMATES: $\mathrm{TMI_{v5}}$, $\mathrm{TMI_{v6}}$, $\mathrm{PR_{v5}}$, AND $\mathrm{PR_{v6}}$

Version-5 and version-6 monthly satellite rain estimates for the TMI and PR were obtained at a gridded resolution of 0.5°. Table 1 defines the monthly rain parameters used in this study, providing information on the TRMM data products and method used to compute each parameter. Orbital track information for each TRMM rain sensor—important in the subsampling of ground data—was obtained from level RG2A12 and RG2B31 georegional gridded rain products produced by the Goddard Distributive Active Archive Center for the Melbourne ground validation (GV) site. The geographical resolution of these products is 0.5° for the TMI and 0.1° for the PR. All of the subsampling of the ground data was performed at the 0.5° scale.

b. Radar and gauge monthly estimates

1) R_0 AND G_0

A 5-yr climatological time series of radar and gauge data was used to validate TMI and PR monthly rain estimates independently. For each satellite sensor (TMI or PR), the two ground-based monthly rain estimates r_0

TABLE 1. Validation and satellite rain parameter definitions.

Rain estimate (symbol)	Instrument	TRMM rain product	Monthly rain estimate (method)
G_0	Gauge	2A56	Continuous integration of 2A56 time series
G_{TMI}	Gauge	2A56	Unconditional monthly rain rate as determined from TMI sampling statistics
G_{PR}	Gauge	2A56	Unconditional monthly rain rate as determined from PR sampling statistics
R_0	Radar	3A54	Continuous integration of 2A53 time series
R_{TMI}	Radar	2A53	Unconditional monthly rain rate as determined from TMI sampling statistics
R_{PR}	Radar	2A53	Unconditional monthly rain rate as determined from PR sampling statistics
TMI_{v5}	TMI	3B31	TRMM monthly rain estimate for TMI at 0.5° resolution using version-5 TMI rain algorithm
TMI_{v6}	TMI	3G68	TRMM monthly rain estimate for TMI at 0.5° resolution using version-6 TMI rain algorithm
PR_{v5}	PR	3A25	TRMM monthly rain estimate for PR at 0.5° resolution using version-5 PR rain algorithm
PR_{v6}	PR	3G68	TRMM monthly rain estimate for PR at 0.5° resolution using version-6 PR rain algorithm

and r_S, as defined in the previous section, were computed from each of the two validation datasets. Refer to Table 1 for descriptions of the radar and gauge ground-based rain parameters used in this study.

The radar and rain gauge data were obtained from the National Weather Service (NWS) Next-Generation Weather Radar (NEXRAD) at Melbourne and were processed by the TRMM Satellite Validation Office (TSVO) at the National Aeronautics and Space Administration (NASA) Goddard Space Flight Center (Wolff et al. 2005). TRMM level-2 and level-3 radar rain products are provided at 2-km^2 resolution and cover a spatially continuous circular region with a radius of 150 km from the Melbourne radar. The 3A54 monthly rain maps provided rain estimates for r_0. This operational TRMM GV product is generated from the instantaneous level-2A53 rain maps using a method of simple time-step integration, which forward integrates the instantaneous rain rates based on the time differences between consecutive radar scans. The level-2A53 operational products generate rain-rate information using the probability matching method developed by Rosenfeld et al. (1994).

The amount of time that the radar is down for maintenance is perhaps the most significant source of error in the radar's estimation of rainfall. Missing radar data only affect the derivation of r_0 when the missing scans contain areas of rain within the radar's sampling domain. The derivation of r_S, on the other hand, is affected any time the satellite is overhead while the radar is down, regardless of whether it is raining (i.e., r_S is determined from unconditional rain statistics).

During data processing, TSVO computes radar downtime as the time difference between any two consecutive scans that are separated by more than 10 min. Table 2 lists radar downtime statistics for the Melbourne radar, as determined by TSVO for all 5 yr of the study. Downtimes vary from 5.5% to 10.5%, with the most downtime reported in 1998 during the Melbourne radar's early years of operation. Note that when the radar is operating in clear-air mode consecutive scans often occur 11–12 min apart, in some cases significantly increasing the apparent radar downtime. The radar downtime shown for the Melbourne radar is about the same as other primary TRMM GV radars (http://trmm-fc.gsfc.nasa.gov/trmm_gv/gv_products/level_2/missing_data.html).

Gauge estimates G_0, G_{TMI}, and G_{PR} were produced from level-2A56 rain products using tipping-bucket data (resolution ~0.01 inches per tip) from 100 gauges received by TSVO from three different gauge networks: the St. Johns Water Management District (STJWMD), South Florida Water Management District (SFWMD), and the Kennedy Space Center (KSC). The number of gauges available in each 0.5 grid box shown in Fig. 1 is displayed in Table 3. The level-2A56 products provide 1-min rain rates using a cubic spline routine to produce a continuous time series at 1-min resolution from a discrete time series of tips.

2) R_{TMI}, R_{PR}, G_{TMI}, AND G_{PR}

The subsampled gridded monthly rain estimates for the radar (R_{TMI} and R_{PR}) and gauges (G_{TMI} and G_{PR})

TABLE 2. Radar downtime (h yr^{-1} and % yr^{-1}).

Year	Radar downtime (h)	Radar downtime (%)
1998	922	10.5
1999	483	5.5
2000	573	6.5
2001	664	7.6
2002	740	8.4

TABLE 3. Number of gauges in each 0.5° cell.

Cell No.	No. of gauges
1	5
2	4
3	23
4	0
5	0
6	10
7	12
8	0
9	0
10	2
11	12
12	0
13	0
14	8
15	21
16	6
Total	100

were first determined at the 0.5° scale using the level-2A53 and level-2A56 rain products, respectively. A mean rain rate was computed for each ground sensor during satellite overpasses. In this study, if the sensor's FOV only covered part of the grid box (i.e., $A_i \leq A$), then the retrieved rain rate s_i associated with A_i was assumed to be the representative rain rate for all of A.

The subsampling of the radar and gauge data was treated differently because of differences in their sampling characteristics. In the radar case, the spatial sampling is continuous across the sampling domain of the radar, and so a ±10-min time window around the overpass time was chosen to ensure the selection of at least one radar scan for each satellite overpass (and never more than two).

Gauge spatial sampling errors depend on the number density and configuration of rain gauges situated in each grid box (Morrissey et al. 1995). As can be seen in Fig. 1, the gauges are unevenly distributed across the study region, with a significant fraction of the overall gauge population situated along the eastern coast of Florida. To compensate in part for the additional spatial sampling uncertainty associated with spatially averaging a nonhomogeneous network of point gauge estimates, a ±30-min time window was used for gauges, theoretically estimated by Bell and Kundu (2003). They assumed a homogenous gauge distribution with a mean separation of about 40 km. With a time window of this size, each gauge in the grid box is effectively treated as an independent rain estimate for the whole box at the overpass time, with the average rain rate computed from all the independent gauge estimates in each box.

3) GAUGE CORRECTION TO RADAR-SUBSAMPLED ESTIMATES R_{TMI} AND R_{PR}

As noted above, there were times when the NWS Melbourne radar was not operating while the satellite was directly overhead. In this case, the number of subsampled radar observations for the month is then less than the total number of satellite overpasses. The method described in section 2 depends on the sampling statistics of the subsampled ground sensor exactly matching the satellite overpass statistics, because otherwise the satellite sampling error cannot be considered to be equivalent to the sampling error for the subsampled ground sensor.

Although radar downtime was not found to be a major issue, the radar sampling statistics were corrected by substituting the mean gauge rain rate for those overpass times when the radar was down while the satellite was overhead. The first step was to create a list of times at which both the satellite was overhead and the Melbourne radar was down. The gauge data were then subsampled at these particular times and the mean overpass rain rates computed were used to update the subsampled time series for the radar. Figures 2a,b show the regression lines for the uncorrected subsampled monthly rain estimates for the radar (R_{TMIunc} and R_{PRunc}) versus the gauge-corrected radar rain estimates for each satellite rain sensor (R_{TMI} and R_{PR}). These scatter diagrams confirm that the correction is very small and that radar downtime was not a significant problem.

4. Florida rainfall climatology

a. *Interannual, intra-annual, and diurnal cycles*

Mesoscale convective storm events contribute up to 40% of Florida's annual rainfall budget (Shepard et al. 2001). These rain events produce very intense rain rates over relatively small areas and are most frequently observed during the summer months, with more thunderstorm days observed in central Florida than anywhere else in the United States (Williams et al. 1992). Florida convection occurs most frequently in the afternoon hours in conjunction with the Florida sea breeze, resulting in the formation of convergence zones. Organized tropical storms and wintertime midlatitude frontal systems also make significant contributions to Florida's annual rainfall budget.

This section examines interannual, intra-annual, and diurnal climatological rain profiles constructed from the 10 different ground-based and satellite rain parameters defined in Table 1. Figures 3a,b display annual rainfall amounts for each year of the study for the TMI-

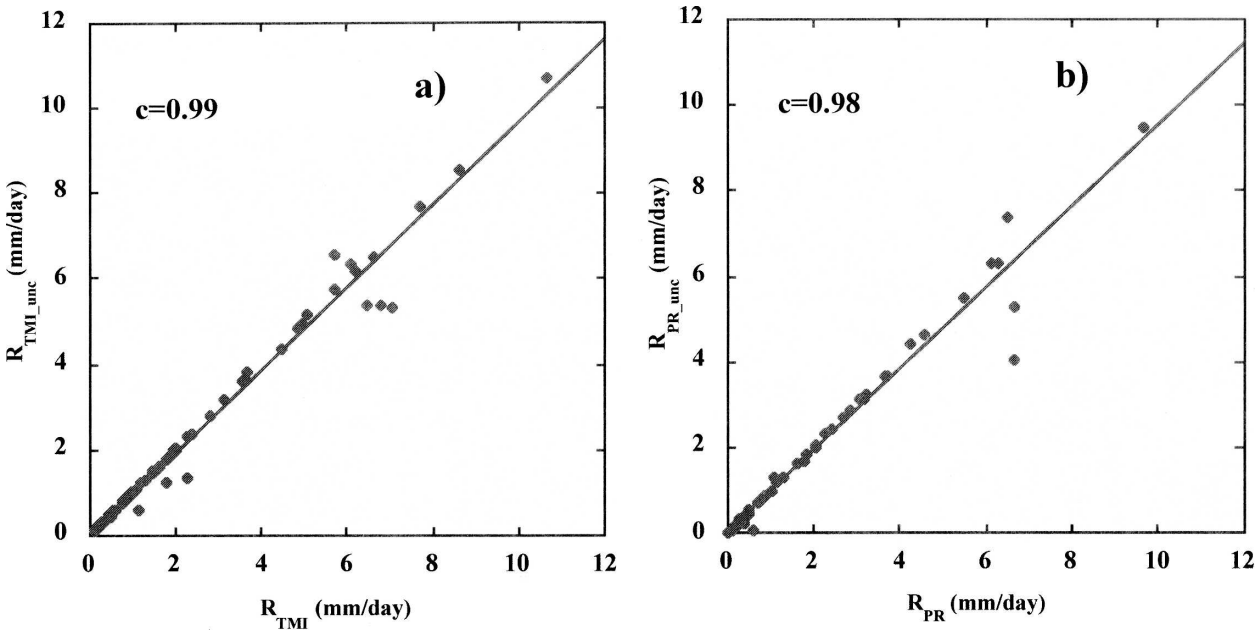

FIG. 2. Scatter diagrams that compare corrected and uncorrected subsampled radar estimates based on field of view for (a) TMI and (b) PR. Radar undersampling was corrected using gauge estimates for TRMM overpasses when the radar was down. The correlation coefficient c is also shown at top left in (a) and (b).

and PR-related rain parameters, respectively. These parameters can be compared with the empirical ground-based references R_0 and G_0, which are plotted in both figures. Both figures reveal a high degree of correlation between satellite and ground sensors, and most of the rain parameters appear to be in good quantitative agreement. In Fig. 3a, it can be seen that TMI_{v5} greatly exceeds the other five rain parameters for every year of this study. The TMI_{v6} profile, on the other hand, is both highly correlated and in reasonably good agreement with the gauge- and radar-derived rain parameters. Overall, there appears to be more variance between the PR rain parameters shown in Fig. 3b. Still, the PR_{v6} annual rainfall remains in relatively close agreement with G_0, R_0, and G_{PR}. Of interest is that the subsampled radar rain estimates R_{TMI} and R_{PR} show the least amount of annual rainfall relative to the other parameters, which is especially salient in the case of R_{PR}. This observation will be discussed in more detail in section 5.

Figures 3c,d display the annual rain anomalies relative to the 5-yr climatological mean rainfall for each rain estimate listed in Table 1. It is observed that negative rainfall anomalies occurred in the year 2000 for all of the rain parameters shown in the two figures. TMI-dependent rain parameters, as well as R_0 and G_0, all exhibit positive anomalies in the other four years. In the case of the PR, very small negative anomalies are observed for PR_{v5} and PR_{v6} in 1998 and 2001 and for G_{PR} and R_{PR} in 2001.

Figures 4a,b compare the intra-annual rain profiles for the ground-based and satellite-inferred rain estimates based on the 5-yr monthly averages computed over the whole study period. It is assumed that R_0 and G_0 profiles represent the best intra-annual climatological description. Figure 4a shows that to the TMI_{v5} annual rainfall far exceeds the other sensors between May and September. The rain budget during these months, as noted earlier, is dominated by strong convective storms. This excess seasonal rainfall clearly contributes to the large differences in the interannual rainfall observed for TMI_{v5} seen in Fig. 3a. The intra-annual rain profile for TMI_{v6} shows better agreement with the other sensors but also exceeds the ground-based rain estimates during the peak months of July and August. Figure 4b, like Fig. 3b, reveals a greater relative separation between each of the curves associated with the PR. These variations are attributed to the additional sampling variance associated with the PR sampling statistics.

Diurnal rain profiles are displayed in Figs. 5a,b for all rain estimation parameters listed in Table 1. Each figure exhibits a normalized diurnal rain profile computed from data collected over the entire 5-yr study period. The rain profiles for each parameter display a large amplitude that is in phase with Florida's afternoon con-

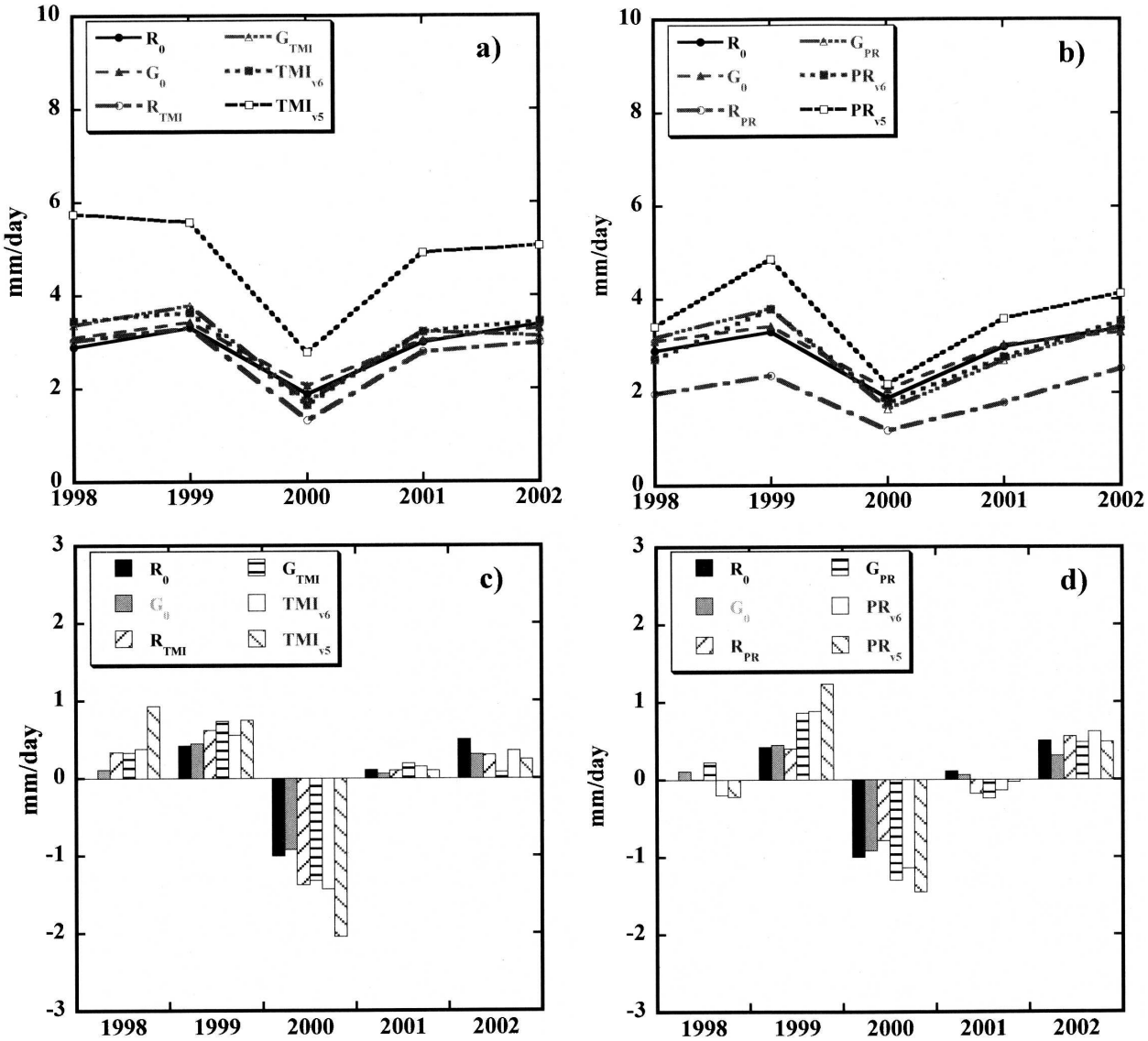

FIG. 3. Five-year interannual rain climatology for Florida, comparing validation and satellite rain parameters for (a) TMI and (b) PR. Also shown are the annual rain anomalies from the 5-yr climatological mean for (c) TMI and (d) PR.

vective cycle. The fraction of rainfall observed for each of the rainfall parameters listed in Table 1 in the time window between 1200 and 1800 eastern standard time (EST) accounts for between 40% and 65% of the total diurnal rain budget. Note that R_0 and G_0 rain profiles display very little structure outside of this period and are completely dominated by the convective cycle. In contrast, TMI_{v6}, TMI_{v5}, and PR_{v6} profiles (instantaneous PR_{v5} data were not available) show some additional climatological structure at other times of the day, with secondary peaks observed at 0300, 0800, and 2100–2200 EST. These relative maxima are in phase with maxima observed in the subsampled profiles of R_{TMI}, G_{TMI}, R_{PR}, and G_{PR}. This fine structure is considered to be a by-product of the satellite's discrete temporal sampling and not to be due to retrieval anomalies.

b. *TRMM's sampling of Florida's diurnal cycle*

The TRMM satellite flies in sun-asynchronous orbit that samples regional rainfall at different times of the day. The frequency and timing of TRMM satellite overpasses on regional scales vary with latitude, with anywhere from one to three observations collected per day. On average, it takes about 46 days for the satellite to collect samples for every hour of the 24-h diurnal cycle (Negri et al. 2002). Near the equator, the sampling interval is approximately constant ($\Delta t \sim 12$ h), whereas

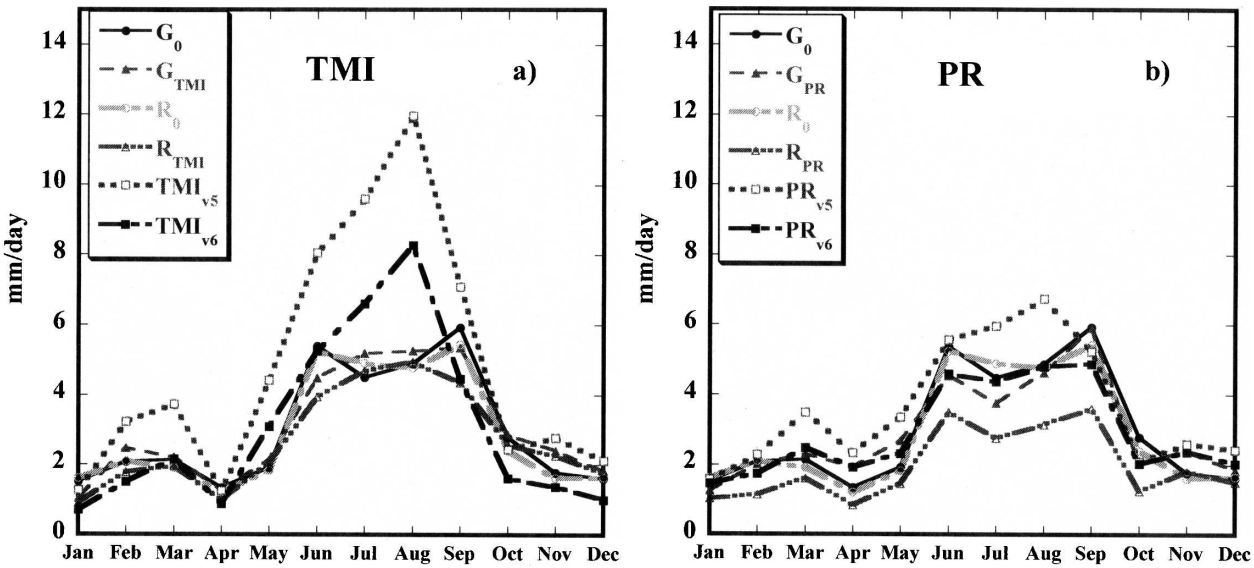

FIG. 4. Intra-annual rain climatological profile for each of the rain parameters listed in Table 2, computed using data from the five study years corresponding to (a) TMI and (b) PR. The R_0 and G_0 are included as empirical references and are used to represent the true rain climatology.

more sampling modes are observed at higher latitudes. Over Florida, three primary sampling frequency modes were identified that correspond to the time intervals $\Delta t = 4.8$, 6.4, and 17.9 h, and two less frequent secondary modes were identified that correspond to $\Delta t = 24.4$ and 29.2 h.

Plots of the 5-yr diurnal sampling statistics for central Florida are shown in Fig. 6 for both the TMI and the PR, where the total number of sensor-dependent observations is plotted as a function of the local hour. The diurnal profile computed for G_0 (also shown in Fig. 5) and a purely oceanic rain profile computed from a gauge network at Kwajalein in the Marshall Islands are also shown in the figure to illustrate the correspondence between TRMM's sampling and the observed diurnal climatology.

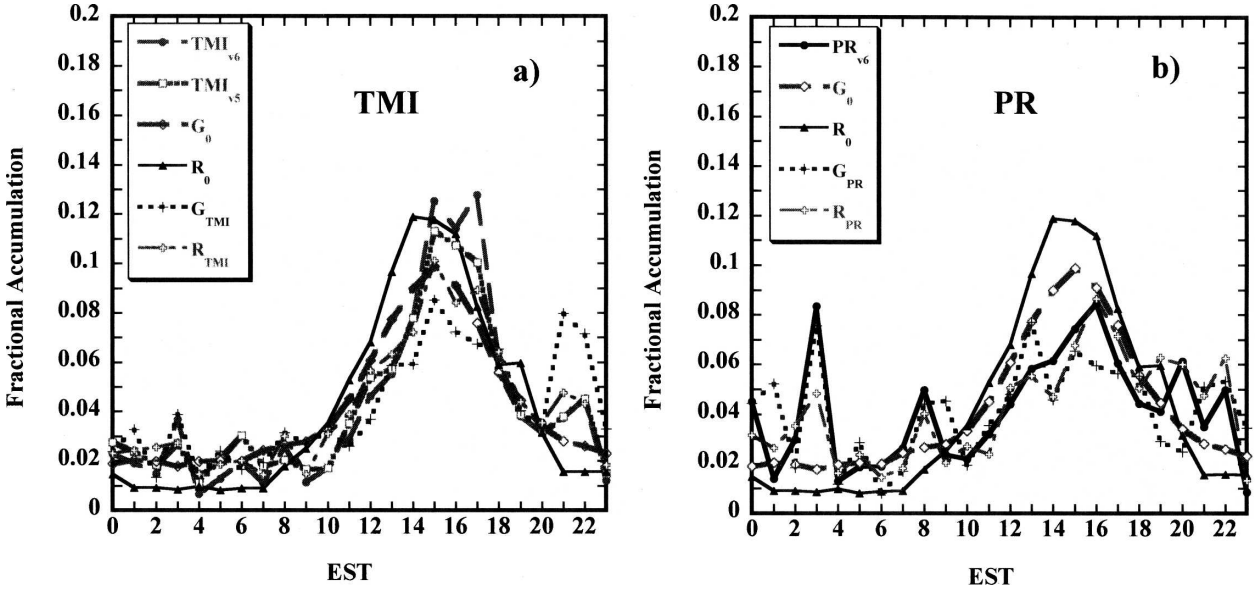

FIG. 5. Diurnal profiles for (a) TMI and (b) PR that compare the different rain parameters used in the study. The PR_{v5} is not shown because the rain-rate information for this parameter was not available.

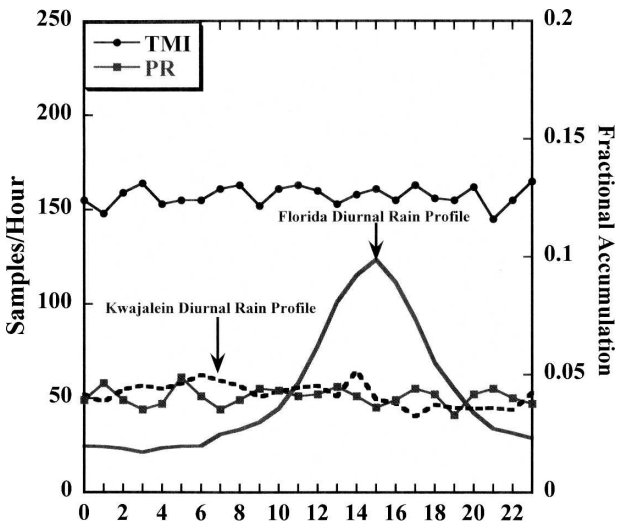

FIG. 6. Diurnal sampling statistics for the TMI and PR. The plot associated with the left *y* axis shows the total number of overpasses per hour over the 5-yr study period as a function of the local time, and the plot associated with the right *y* axis shows normalized diurnal rain profiles for Florida and Kwajalein.

Figure 6 shows that, when considered over a sufficiently long time period at a spatial resolution of 0.5°, the sampling rate per hour is roughly constant for both rain sensors, averaging about 30 observations per hour per year for the TMI and about 10 for the PR. It is clear that this sampling scenario would be considered to be fairly ideal for an oceanic region like Kwajalein; however, Florida's diurnal rain budget receives the bulk of its rainfall within a time window extending from the late morning to the early evening. This relationship between sampling and climatology will be further discussed in subsequent sections.

5. Statistical evaluation of the radar–rain gauge parameters

a. Radar–rain gauge correlations

The monthly radar and gauge estimates used in this study to generate regional error statistics for the TMI and PR rainfall estimates have different spatiotemporal error characteristics. This section investigates the correlation structure and variance differences of the radar and gauge rain parameters to gain insight into the strengths and weaknesses of each ground-based rain sensor used in the validation of TRMM satellite estimates for the area shown in Fig. 1.

The tipping-bucket rain gauge estimates rainfall directly at a discrete point location by counting and time stamping the fixed volume increments of rainwater collected inside its 8-in. circular orifice. A tipping-bucket rain gauge incurs measurement uncertainties related to the mechanics of its operation and its ambient surroundings (Groisman and Legates 1994). Furthermore, gridded gauge estimates determined from a collection of gauges within some areal region incur spatial sampling errors due to uncertainties associated with the physical separation of the individual gauges in the grid box (Morrissey et al. 1995). The radar, in contrast, collects rain information over a large geospatial field continuum. However, the radar, unlike the rain gauge, does not directly measure precipitation at the surface but rather measures reflectivity aloft. Surface rain rates are subsequently inferred from the empirical relations between reflectivity and rain rate (Wilson and Brandeis 1979).

Studies that compare rain estimates derived from radar and gauges typically show large random errors at instantaneous scales (Zawadzki 1975; Habib and Krajewski 2002). Zawadzki (1975) showed that random and systematic errors between radar and gauge rain rates resulted from differences between the spatiotemporal error characteristics of the two sensors. Zawadzki argued that these random errors could be minimized by optimally averaging the instantaneous radar and gauge measurements in space and time, respectively. Ciach and Krajewski (1999) developed a statistical method that relates the relative radar–rain gauge variance difference to the absolute error variance of the radar and gauge (i.e., estimated relative to the true rainfall). Habib and Krajewski (2002) used the method of Ciach and Krajewski (1999) and applied it to radar and gauge data from central Florida. They showed that significant random errors existed between the instantaneous rain rates from these two ground-based sensors but that as the integration time was increased the error variance decreased.

Figures 7a,b display scatter diagrams that compare the subsampled rain estimates with the primary empirical references: R_{TMI} and R_{PR} versus R_0, and G_{TMI} and G_{PR} versus G_0, respectively. The validation rain parameters R_{TMI} and G_{TMI} are more highly correlated with R_0 and G_0 than are R_{PR} and G_{PR}. This expected result can be attributed to the TMI's larger FOV, which yields more observations per month for the TMI as compared with the PR (see Fig. 6). More important is that in Fig. 7a it can be seen that the two regression lines appear to be negatively biased relative to R_0. The subsampled gauge rain parameters shown in Fig. 7b, on the contrary, do not appear to be biased relative to G_0.

The scatter diagrams shown in Figs. 7c,d compare radar and gauge rain parameters corresponding to the same sampling statistics: R_{TMI} versus G_{TMI}, R_{PR} versus G_{PR}, and R_0 versus G_0. The empirical references R_0 and

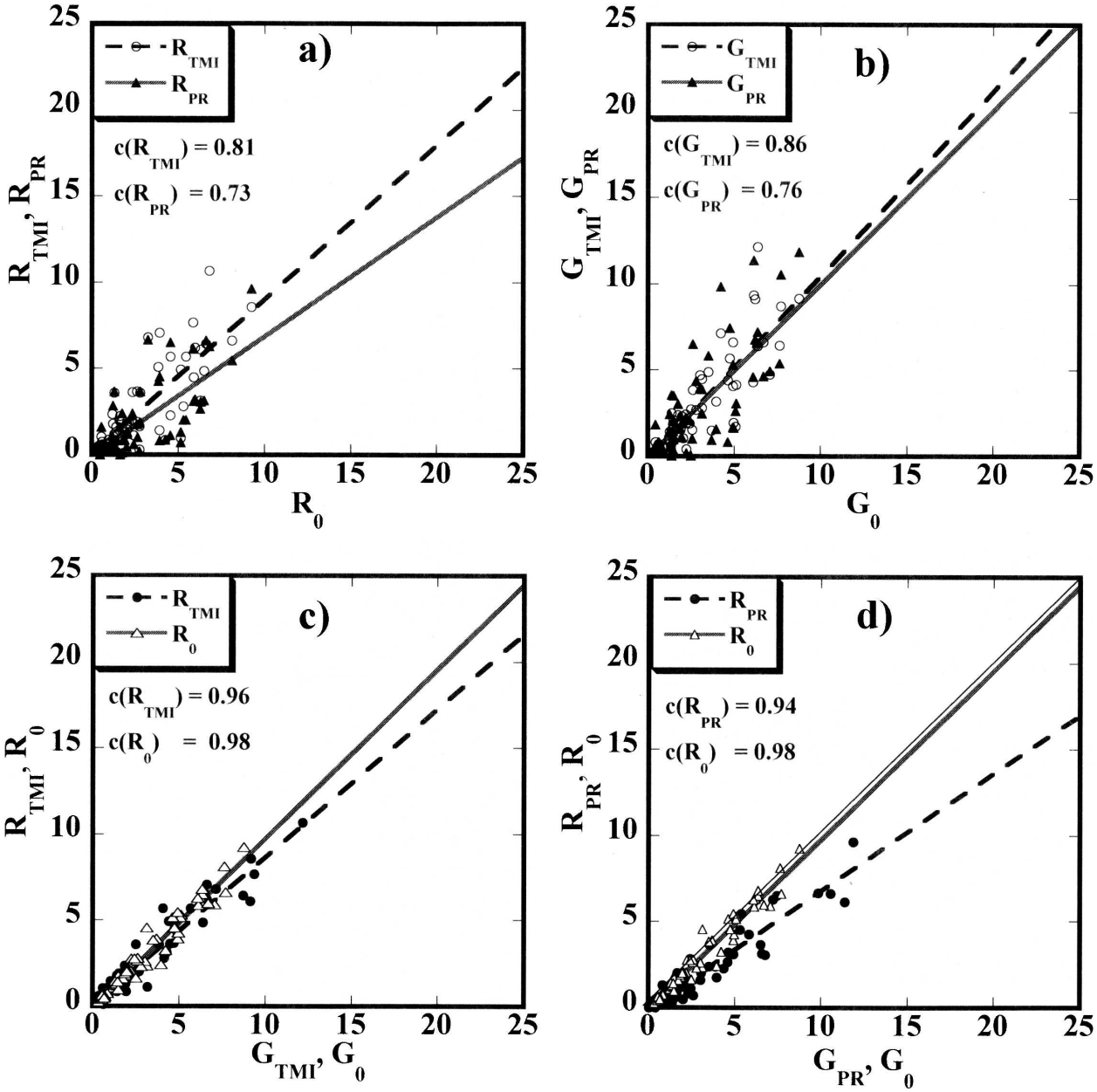

FIG. 7. Scatter diagrams showing radar–gauge monthly rain estimates for (a) R_{TMI} and R_{PR} vs R_0, (b) G_{TMI} and G_{PR} vs G_0, (c) R_{TMI} vs G_{TMI} and R_0 vs G_0, and (d) R_{PR} vs G_{PR} and R_0 vs G_0. Correlation coefficients for each regression are shown below the plot legend. The unit for each axis is millimeters per day, and the sample size for each plot is 60.

G_0 appear to be highly correlated and are nearly unbiased. The corresponding subsampled radar and gauge estimates are also highly correlated but reveal the existence of a negative radar subsampling bias that is nearly linear. A bias-correction factor for R_{TMI} and R_{PR} was computed using the slope parameters derived for each regression relative to R_0. This correction was then applied to each of the subsampled radar rain parameters, yielding correction factors of 1.11 and 1.43 for R_{TMI} and R_{PR}, respectively. It is speculated that this bias may relate to differences in the relative sampling frequency of the TMI and PR.

Salby and Callaghan (1997) show that satellite undersampling can statistically bias the inferred mean diurnal profile. An examination of Fig. 5 shows that all four subsampled rain parameters, R_{TMI}, R_{PR}, G_{TMI}, and G_{PR}, undersampled Florida's peak convective period relative to the R_0 and G_0 profiles. These profiles indi-

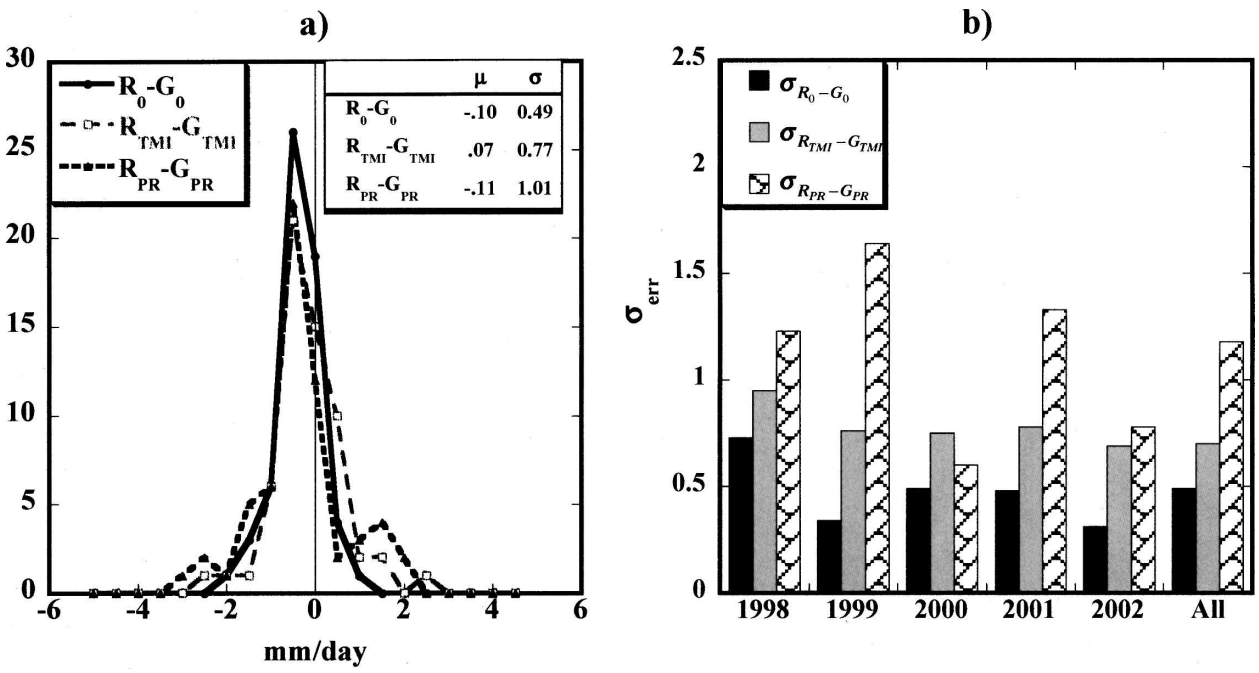

FIG. 8. (a) Radar–gauge *error* distributions for continuous and subsampled monthly rain estimates. The first two statistical moments (mm day^{-1}) are displayed in the small box on the right-hand side. (b) The annual rsme estimates for $\sigma_{R_0-G_0}$, $\sigma_{R_{\mathrm{TMI}}-G_{\mathrm{TMI}}}$, and $\sigma_{R_{\mathrm{PR}}-G_{\mathrm{PR}}}/\sigma_{R_0-G_0}$.

cate that a higher fraction of the subsampled diurnal rainfall occurred at other times of the day, outside the peak convective period observed in Fig. 5. When considered on monthly scales, however, Fig. 7b, in contrast, shows no evidence of a strong bias for G_{TMI} and G_{PR} with respect to G_0. Systematic undersampling of the diurnal cycle, therefore, does not explain the source of the subsampling bias observed in R_{TMI} and R_{PR}.

The measurement field of the radar, as noted above, is spatially continuous, whereas for the rain gauge network it is spatially discrete. These sampling differences should have a direct effect on the mean unconditional statistics that determine the subsampled gridded estimates for the radar and gauges. Because the radar sampling is continuous, the mean statistics include the complete set of rainy and nonrainy pixels that cover the areal dimensions of the grid box. The subsampled gauge estimate, however, depends only on the number of independent gauges in the grid box (it is assumed that all of the gauges produce independent measurements, i.e., are physically separated by a distance that exceeds the correlation distance). These sampling differences may be coupled with differences in the autocorrelation function observed for each sensor at the 0.5° scale. We consider these sampling issues affecting the mean unconditional statistics—possibly in conjunction with the radar's undersampling of the diurnal cycle's peak phase—as the most likely source of the radar subsampling bias.

b. Radar–rain gauge error statistics

Figure 8a displays three distributions representing the relative differences between the monthly radar and gauge rain estimates for both continuous and subsampled cases (i.e., $R_0 - G_0$, $R_{\mathrm{TMI}} - G_{\mathrm{TMI}}$, and $R_{\mathrm{PR}} - G_{\mathrm{PR}}$). Each distribution was binned at 1.0 mm day^{-1} intervals and a bias correction was applied to R_{TMI} and R_{PR}. The first two statistical moments for each distribution are shown in the small table that appears on the right side of Fig. 8a. Each of the three distributions appears relatively symmetrical with respect to the mode, which in each case is negative. The relative $R_0 - G_0$ errors are moreover distributed within a narrow range about zero. The other two distributions display a broader dynamic range of values relative to $R_0 - G_0$, as indicated by the standard deviations in each case. These differences are consistent with the temporal sampling of the TMI and PR. In applying their error-variance separation method, Ciach and Krajewski (1999) relate the relative radar–gauge variance to the absolute standard errors (relative to r_T) for each sensor. In this study, we will only evaluate the relative radar–gauge variance.

The standard errors associated with each error distribution were computed for each year of the study and are displayed in Fig. 8b. This figure further illustrates the effects that discrete temporal sampling has on the climate-scale error statistics. The standard deviations $\sigma_{R_{\mathrm{PR}}-G_{\mathrm{PR}}}$ and $\sigma_{R_{\mathrm{TMI}}-G_{\mathrm{TMI}}}$ significantly exceed $\sigma_{R_0-G_0}$ in all five years. Also, $\sigma_{R_{\mathrm{TMI}}-G_{\mathrm{TMI}}}$ exceeds $\sigma_{R_{\mathrm{PR}}-G_{\mathrm{PR}}}$ in all years but 2000, which was an anomalously dry year.

6. Climatological validation of TRMM monthly rain estimates

a. Satellite–ground correlations

Subsampled ground-based estimates of monthly rainfall provide the critical rain information used to decompose the sampling and retrieval errors from the total error in TMI and PR monthly rainfall estimates. Because the subsampled rainfall estimates are assumed to include the temporal sampling error of the satellite, they can also be effectively used to statistically probe the TMI and PR retrieval errors.

Scatterplots that compare TMI and PR monthly rainfall estimates with gridded, subsampled rain estimates from the radar and gauges are shown in Fig. 9. The monthly rain estimates R_{TMI} and R_{PR} were first bias adjusted by applying the bias correction computed in the previous section. It is observed that TMI and PR monthly rainfall estimates are highly correlated with all four of the subsampled rain parameters, R_{TMI}, R_{PR}, G_{TMI}, and G_{PR}. The correlations in the case of the PR are noted to be slightly higher than similar correlations for the TMI. $\mathrm{TMI}_{\mathrm{v5}}$ monthly estimates also exhibit a positive retrieval bias, which is not observed for $\mathrm{TMI}_{\mathrm{v6}}$. The relatively high correlations shown in Fig. 9 are encouraging and show reasonably good quantitative agreement between satellite and subsampled ground estimates.

b. Error distributions

Error distributions that characterize TMI and TRMM PR total, sampling, and retrieval errors are displayed in Figs. 10a–f. The errors computed for each month of the study were binned at 1.0 mm day^{-1} resolution and included 60 samples that cover the 5-yr study period. The first two statistical moments parameterizing each distribution can be found in Table 4. Note that the TMI and PR sampling error distributions were completely determined from the validation datasets, as described earlier in section 2.

Radar- and gauge-inferred sampling errors are shown in Figs. 10c,d for the TMI and PR, respectively. Both are in good agreement and approximate normal distributions consistent with the central limit theorem. The PR sampling error distributions are broader than similar distributions computed for the TMI, which, as previously noted, can be related to differences in the relative sampling characteristics of the TMI and the PR sensors.

The TMI retrieval error distributions shown in Fig. 10e, in contrast, tend to be broader and more positively skewed than the corresponding error distributions for the PR shown in Fig. 10f. An examination of the standard deviations listed in Table 4 further indicates that regional retrieval errors have been reduced in version-6 products for both the TMI and PR, though the improvements in the TMI are more prominent. Note also that seven of the eight distributions in Figs. 10e,f have a slightly negative mode, a point that will be discussed in more detail shortly. The TMI retrieval error distribution in Fig. 10e appears to be positively skewed, indicating the presence of large positive retrieval errors. The PR retrieval errors are also more narrowly distributed, and overall the shape appears more Gaussian.

The PR and the TMI estimates of the mean rainfall include contributions from the true rainfall and the total error. The total error distributions for the TMI and PR display a relative high frequency of small negative errors combined with the relative low frequency of large positive errors that results in an intrinsic skewness in the shape of each distribution. However, when averaged over the entire study period, the mean error still converges on zero (see Table 4 and note that the large positive mean error observed for $\mathrm{TMI}_{\mathrm{v5}}$ indicates the presence of a positive bias). This statistical property, which was also observed in an earlier regional study of Oklahoma by Fisher (2004), seems to be a fundamental characteristic of the total error distribution.

Morrissey and Janowiak (1996) also reported similar findings. In their earlier study, they subsampled geosynchronous IR pentads over eight different time intervals (0000, 0300, 0600, . . . , 2100) for three different tropical regions. The rainfall estimate computed from the complete time series was used a control. Subsequent regressions of these different sampling scenarios showed a definite trend in which the subsampled data tended to overestimate the large rain events while underestimating the smaller events. The scatterplots revealed the existence of a crossing point at the low end of the rain-rate spectrum in the regressions lines, which subdivided the relative errors into negative and positive regions. They subsequently related these observations to the existence of a conditional sampling bias that varied with rain rate and depended on the averaging scale, the sampling interval, and the autocorrelation structure of the rainfall.

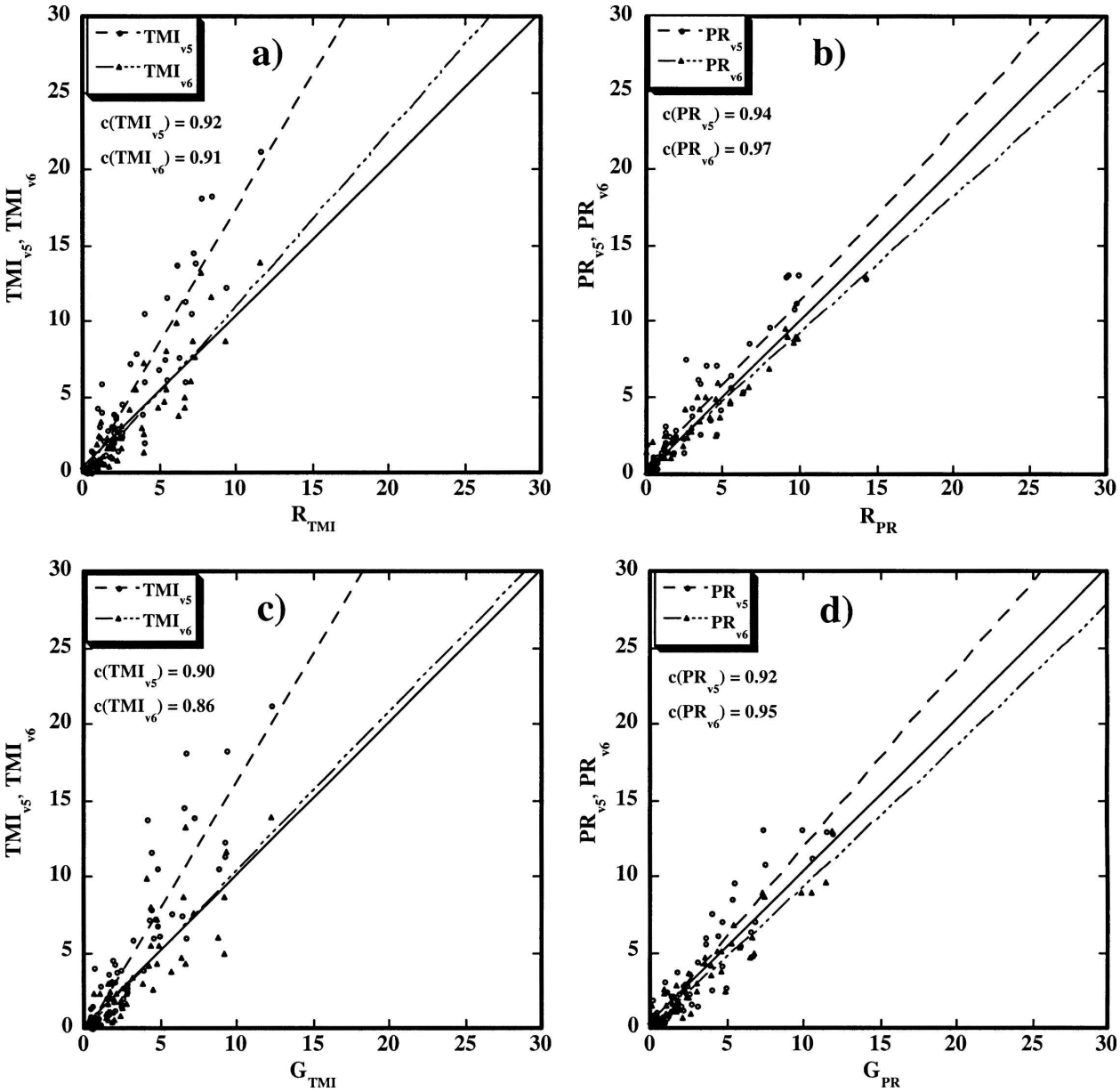

FIG. 9. Scatter diagrams for version-5 and version-6 satellite–ground monthly estimates showing regressions for (a) TMI_{v5} and TMI_{v6} vs R_{TMI}, (b) PR_{v5} and PR_{v6} vs R_{PR}, (c) TMI_{v5} and TMI_{v6} vs G_{TMI}, and (d) PR_{v5} and PR_{v6} vs G_{PR}. The correlation coefficients for the regression lines are shown below the plot legend. The unit for each axis is millimeters per day.

c. *TMI and PR random errors*

Relative sampling and retrievals errors in TMI and PR monthly rainfall estimates were statistically characterized using (12) and (13) described in section 2. The standard errors and the means were also used to compute sampling and retrieval coefficients of variation for each sensor. The coefficient of variation is a useful statistic in performing interannual rainfall comparisons, because it normalizes the standard error relative to the mean, therefore effectively removing the bias associated with the annual variations in the mean rainfall. The sampling and retrieval coefficients of variations are defined as

$$\alpha_{\text{sam}} = \frac{\sigma_{\text{sam}}}{1/2(\mu_{r_0} + \mu_{r_S})} \quad \text{and} \tag{16}$$

$$\alpha_{\text{ret}} = \frac{\sigma_{\text{ret}}}{1/2(\mu_{r_S} + \mu_{s_0})}, \tag{17}$$

where μ_{r_0}, μ_{r_S}, and μ_{s_0} are the annual means computed for r_0, r_S, and s_0, respectively. The denominator repre-

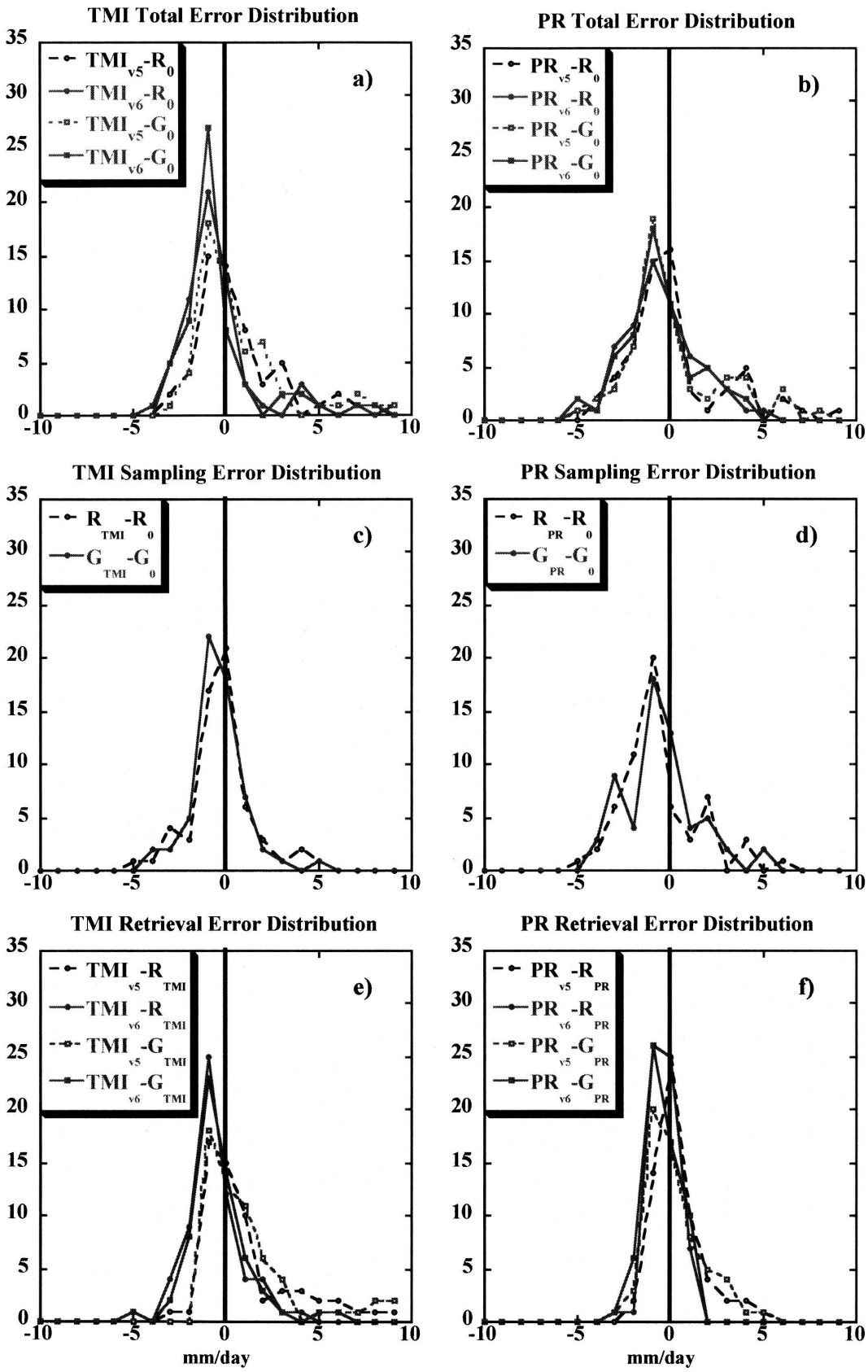
TMI Total Error Distribution
a)
TMI v5 -R 0
TMI v6 -R 0
TMI v5 -G 0
TMI v6 -G 0
PR Total Error Distribution
b)
PR v5 -R 0
PR v6 -R 0
PR v5 -G 0
PR v6 -G 0
TMI Sampling Error Distribution
c)
R TMI -R 0
G TMI -G 0
PR Sampling Error Distribution
d)
R PR -R 0
G PR -G 0
TMI Retrieval Error Distribution
e)
TMI v5 -R TMI
TMI v6 -R TMI
TMI v5 -G TMI
TMI v6 -G TMI
PR Retrieval Error Distribution
f)
PR v5 -R PR
PR v6 -R PR
PR v5 -G PR
PR v6 -G PR
mm/day
mm/day

TABLE 4. First two statistical moments (error mean $\mu_{\rm err}$ and error standard deviation $\sigma_{\rm err}$) for each error distribution shown in Figs. 10a–f.

	Satellite parameter	Validation sensor and rain parameter	$\mu_{\rm err}$	$\sigma_{\rm err}$
Total error	$\mathrm{TMI_{v5}}$	Radar: R_0	1.92	3.74
	$\mathrm{TMI_{v5}}$	Gauge: G_0	1.83	3.68
	$\mathrm{TMI_{v6}}$	Radar: R_0	0.17	2.26
	$\mathrm{TMI_{v6}}$	Gauge: G_0	0.08	2.23
	$\mathrm{PR_{v5}}$	Radar: R_0	0.73	2.68
	$\mathrm{PR_{v5}}$	Gauge: G_0	0.64	2.63
	$\mathrm{PR_{v6}}$	Radar: R_0	0.02	1.97
	$\mathrm{PR_{v6}}$	Gauge: G_0	−0.07	1.93
Sampling error	TMI	Radar: R_0, $R_{\rm TMI}$	0.22	1.70
	TMI	Gauge: G_0, $G_{\rm TMI}$	0.05	1.44
	PR	Radar: R_0, $R_{\rm PR}$	−0.06	2.11
	PR	Gauge: G_0, $G_{\rm PR}$	−0.05	1.92
Retrieval error	$\mathrm{TMI_{v5}}$	Radar: $R_{\rm TMI}$	1.70	2.75
	$\mathrm{TMI_{v5}}$	Gauge: $G_{\rm TMI}$	1.77	3.68
	$\mathrm{TMI_{v6}}$	Radar: $R_{\rm TMI}$	−0.04	1.45
	$\mathrm{TMI_{v6}}$	Gauge: $G_{\rm TMI}$	0.08	1.73
	$\mathrm{PR_{v5}}$	Radar: $R_{\rm PR}$	0.80	1.34
	$\mathrm{PR_{v5}}$	Gauge: $G_{\rm PR}$	0.69	1.51
	$\mathrm{PR_{v6}}$	Radar: $R_{\rm PR}$	0.08	0.72
	$\mathrm{PR_{v6}}$	Gauge: $G_{\rm PR}$	−0.03	0.91

sents the average of the two rain estimates used in the computation of the standard error.

Figures 11a,b show the annual sampling standard error $\sigma_{\rm sam}$ and sampling error coefficients of variation $\alpha_{\rm sam}$ for the TMI and PR rain estimates. Both statistics indicate that random sampling errors tend to be slightly lower for the TMI than for the PR while exhibiting only a small dependency on the particular validation reference. The 5-yr ratio of PR to TMI standard errors $\sigma_{\rm sam}$ was found to be about 1.26 using the radar as the validation sensor and 1.34 using the gauges. Figure 11b displays a similar trend for $\alpha_{\rm sam}$ as observed in Fig. 11a. Considerably higher values of $\alpha_{\rm sam}$ are observed in 2000, but an anomalously low mean rainfall was observed that year, as can be seen in Figs. 3c,d.

Figures 12a,c provide similar annual error budget estimates for the version-6 TMI and PR estimates. The PR exhibits significantly smaller year-to-year retrieval errors for both error statistics. Considered over the 5-yr period of the study, the ratios of PR to TMI retrieval errors were 0.49 for the radar and 0.52 for the gauges. The smaller retrieval errors observed for the PR are attributed to the superior vertical and horizontal resolutions of the PR, which is better able to resolve the gradients in rain structures associated with mesoscale convective rain systems. The hardware and sampling characteristics of the PR are also more physically similar to the ground radar. TMI's data sampling over land, on the other hand, is limited to the two 85.5-GHz channels, which are most directly correlated with ice-scattering processes occurring above the freezing level (Spencer et al. 1989). Figure 12b displays the version-6-to-version-5 retrieval standard error ratios for the TMI and PR and indicates that TMI and PR retrieval errors have both been reduced by nearly 50% from version 5 to version 6.

d. Satellite versus ground-based standard errors: σ_{sam} and σ_{ret} versus σ_{val}

The random errors in the ground-based reference r_0 are characterized by $\mathrm{var}(r_0 - r_T)$. Kummerow et al. (2000) point out that comparisons between ground-based and satellite rain estimates cannot be used to reduce uncertainties in the satellite estimates below the uncertainties in the validation products, which can range between 10% and 15%. Although the absolute uncertainties in the ground data depend on r_T, an upper bound on r_T can be established using the error variance separation method developed by Ciach and Krajewski (1999). Applying their technique to this study, the relative radar–gauge variance, $\mathrm{var}(R_0 - G_0)$, can be approximated as

$$\mathrm{var}(R_0 - G_0) \approx \mathrm{var}(R_0 - r_T) + \mathrm{var}(G_0 - r_T). \tag{18}$$

To gain some insight into the relative magnitude of $\sigma_{\rm sam}$ and $\sigma_{\rm ret}$ with respect to $\sigma_{\rm val}$, we will treat $\mathrm{var}(R_0 - G_0)$ as an upper bound on $\mathrm{var}(r_0 - r_T)$ appearing in (18).

The following two equations are then used to probe the ratios of satellite to ground-based errors with respect to the three primary error sources in (8):

$$\omega_{\rm sam}(s_0, r) = \sigma_{\rm sam}/\sigma_{R_0 - G_0} \quad \text{and} \tag{19}$$

$$\omega_{\rm ret}(s_0, r) = \sigma_{\rm ret}/\sigma_{R_0 - G_0}, \tag{20}$$

where s_0 corresponds to either the TMI or the PR and r designates the particular empirical reference (radar or

←

FIG. 10. Histograms displaying distributions of (a) TMI total error, (b) PR total error, (c) TMI sampling error, (d) PR sampling error, (e) TMI retrieval error, and (f) PR retrieval error. The above error distributions were determined from monthly satellite and validation rain parameters for the full study region shown in Fig. 1. Note that the sampling errors are independent of the rain algorithm and so are not affected by the version number.

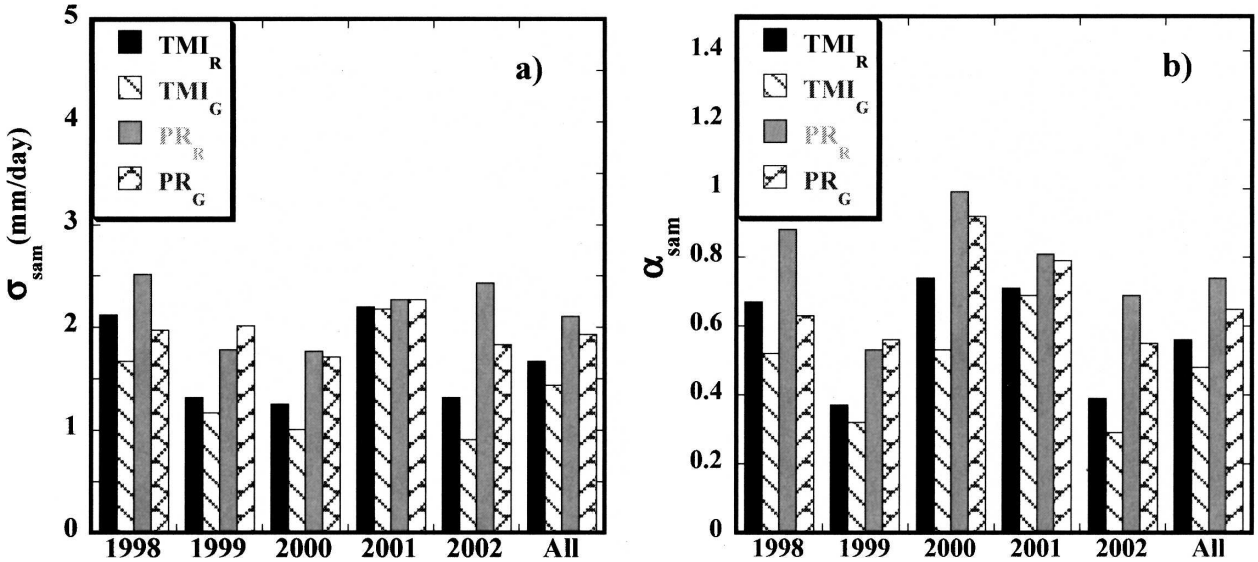

FIG. 11. Version-6 TMI and PR sampling errors showing (a) standard error σ_{sam} and (b) coefficients of variation α_{sam}, for each year of the study. The subscript in each legend designates the ground sensor used to infer the sampling errors (i.e., R for radar and G for gauge).

gauge) used in the determination of σ_{sam} and σ_{ret}. Note that $\sigma_{R_0-G_0}$ does not depend on s_0 or r.

Climate-scale values for ω_{sam} and ω_{ret} were computed annually and are shown in Figs. 13a,b, respectively. Figure 13a shows that ω_{sam} varies between about 2 and 6 from year to year, indicating that the upper bound on σ_{val} is at least a factor of 2 smaller than σ_{sam}. The ω_{sam} values for the PR consistently exceed the corresponding TMI values by an amount proportional to the sampling differences between the two sensors. The TMI and PR values for ω_{ret} shown in Fig. 13b, reveal more pronounced differences between the two sensors, with ω_{ret} values for the TMI consistently greater (by a factor of 2 in several cases) than corresponding values for the PR. Although PR retrieval errors tend to exceed $\sigma_{R_0-G_0}$ by around a factor of 2, Fig. 13b shows that the PR's σ_{ret} approaches the upper bound on σ_{val} in 1998 and 2000. These results all indicate that σ_{val} makes a significant, nonneglible contribution to the total error budget as described in (8).

e. TMI and PR systematic errors (bias)

Systematic errors in version-6 TMI and PR estimates due to sampling and retrievals were computed using (9) and (10) in section 2. The results of these calculations for the TMI and PR are displayed in Figs. 14a,b. TMI and PR sampling biases computed for the radar and the gauge show good agreement when considered on climate scales of a year or more and reveal no definite positive or negative tendency with respect to the temporal sampling of the TRMM satellite. The TMI sampling biases, in contrast with the random errors shown in Fig. 11a, exceed the PR sampling biases in some years. The missing radar data in 1998 may explain some of the large TMI_R sampling bias in that year. TMI_G also exceeds PR_G in 1998, but the difference is relatively small. When averaged over all years, the sampling biases for TMI_R and TMI_G were 6% (radar) and 2% (gauge), respectively, whereas corresponding PR biases were about −2% for both validation sensors.

The sample size (five points) is not large enough to confirm a statistical relationship between sampling and climatology, but natural climatological variability affects the probability of observing rain (i.e., varying frequency distribution), which, in turn, affects the probability of the TMI and PR observing rain during TRMM overpasses, considered over durations of 1 yr or more. In comparing Figs. 3b,c with Fig. 14a, there appears to be a fair degree of correlation between the observed annual rainfall anomaly and the relative sampling bias. This apparent relationship is especially prominent in 2000. Although further study is needed, it may be possible to estimate indirectly the annual sampling biases based on a determination of the rainfall anomaly, possibly combined with other statistical parameters such as rain frequency and mean event duration.

Annual retrieval biases for the TMI and PR are shown in Fig. 14b. These biases tend to be less than 10% and reveal a slight positive tendency overall, with

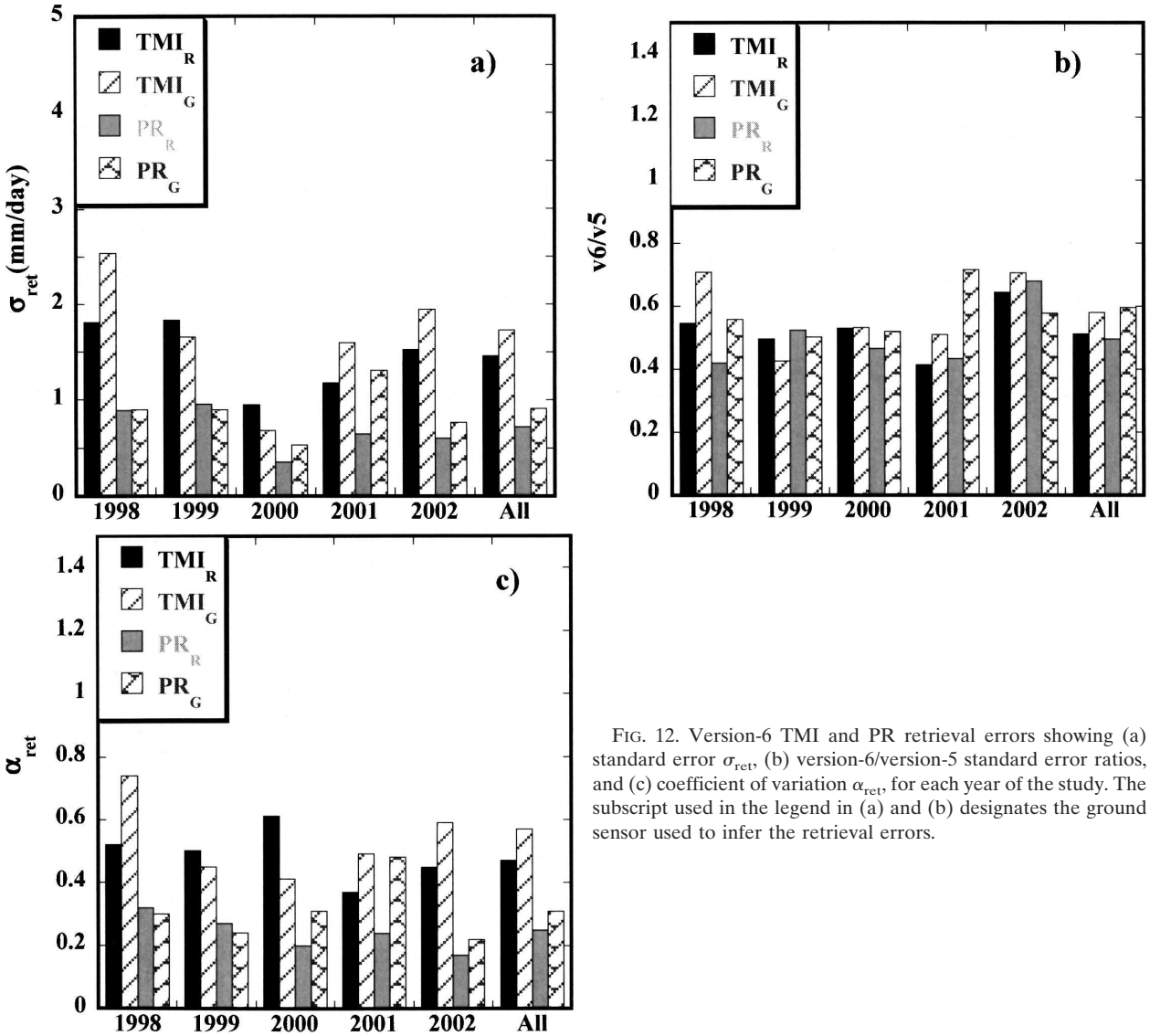

FIG. 12. Version-6 TMI and PR retrieval errors showing (a) standard error σ_{ret}, (b) version-6/version-5 standard error ratios, and (c) coefficient of variation α_{ret}, for each year of the study. The subscript used in the legend in (a) and (b) designates the ground sensor used to infer the retrieval errors.

the radar and the gauges again displaying fairly consistent results. The most notable exception occurred in 1999, when the PR retrieval biases were about −15.8% for the radar-inferred estimate and 0.0% for the gauge-inferred estimate. Furthermore, when considered over all five years of the study, the retrieval biases calculated were all less than 5% and only revealed a small dependence on the validation sensor.

Figures 15a–c display mean monthly sampling and retrieval biases for the TMI and PR estimates for the 5-yr study period. The results in Fig. 15a in general show no evidence of a seasonal sampling bias for either TMI or the PR. A closer examination of Fig. 15a with Fig. 4 reveals that the largest sampling biases tend to occur in the drier months. TMI sampling biases determined from the radar ranged from 0.59 (November) to −0.35 (January), whereas PR sampling biases ranged from 0.60 (November) to −0.26 (February). TMI sampling biases determined from the gauges similarly ranged from 0.35 (November) to −0.32 (January), and for the PR ranged from 0.44 (April) to −0.27 (October).

The retrieval biases for the TMI and PR (versions 5 and 6) are plotted in Figs. 15b,c, respectively. These results reveal some distinct differences between the TMI and PR. Version-5 retrieval biases for both sensors are mostly positive and are greatest during the summer months when the most rainfall is observed. TMI version-5 retrieval biases are seen to be around 100% during the months of May, June, July, and August. Version-6 retrieval biases are also considerably lower than version-5 biases for both the TMI and PR.

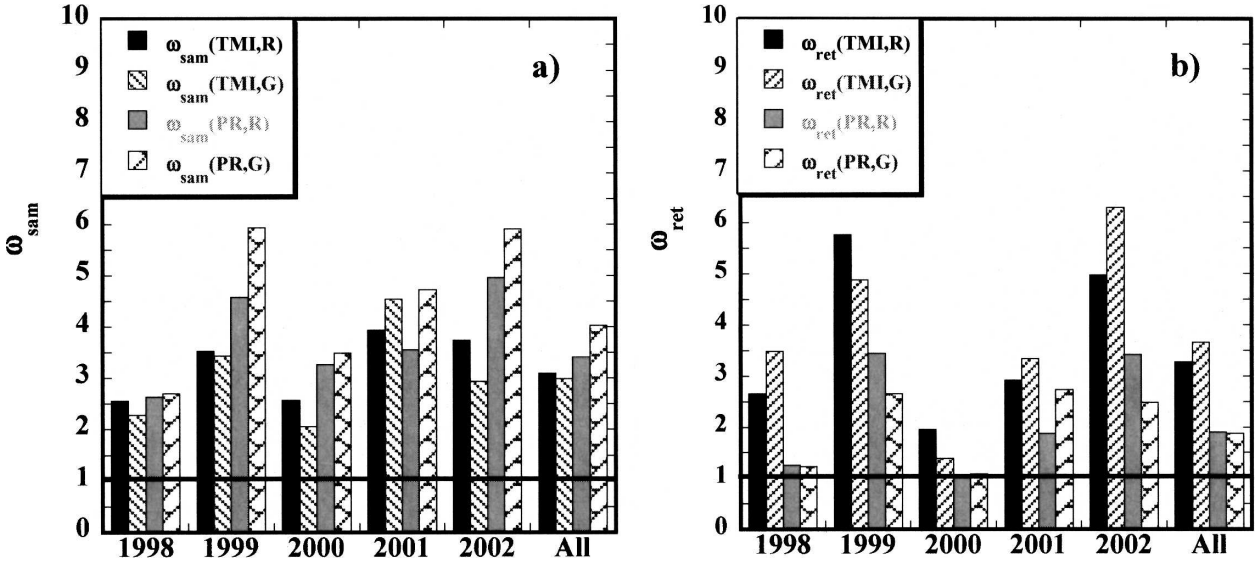

FIG. 13. The (a) ω_{sam} and (b) ω_{ret} for TMI and PR for each year of study.

TMI_{v6} biases, however tend to be negative during the winter months and positive during the summer months, suggesting the presence of a seasonal retrieval bias in which the sign alternates between winter and summer. McCollum et al. (2002) observed this bias in connection with wintertime stratiform precipitation and attributed it to smaller ice-scattering cross sections during the colder months. Fisher (2004) also reported seeing a negative wintertime bias and positive summertime bias in TMI rain estimates over Oklahoma. The PR version-5 retrieval biases shown in Fig. 15c are positive for all months but one (September). The version-6 PR retrieval biases, on the other hand, appear to be more randomly distributed between positive and negative for both validation sensors.

7. Summary and discussion

Regardless of whether the measurements are made from the ground or from space, precipitation is one of the most difficult geophysical variables to measure accurately. In the ideal case, the accuracy of satellite (s_0)

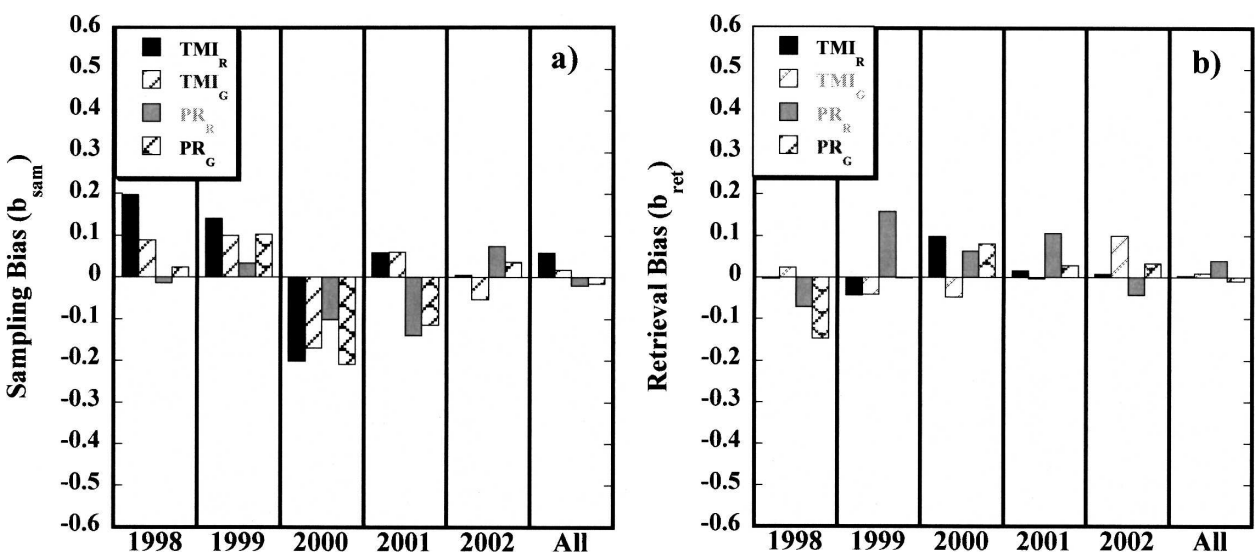

FIG. 14. TMI and PR (a) sampling biases and (b) version-6 retrieval biases as inferred from radar and gauge estimates. The subscript used in the legend designates the ground sensor used to infer the sampling errors.

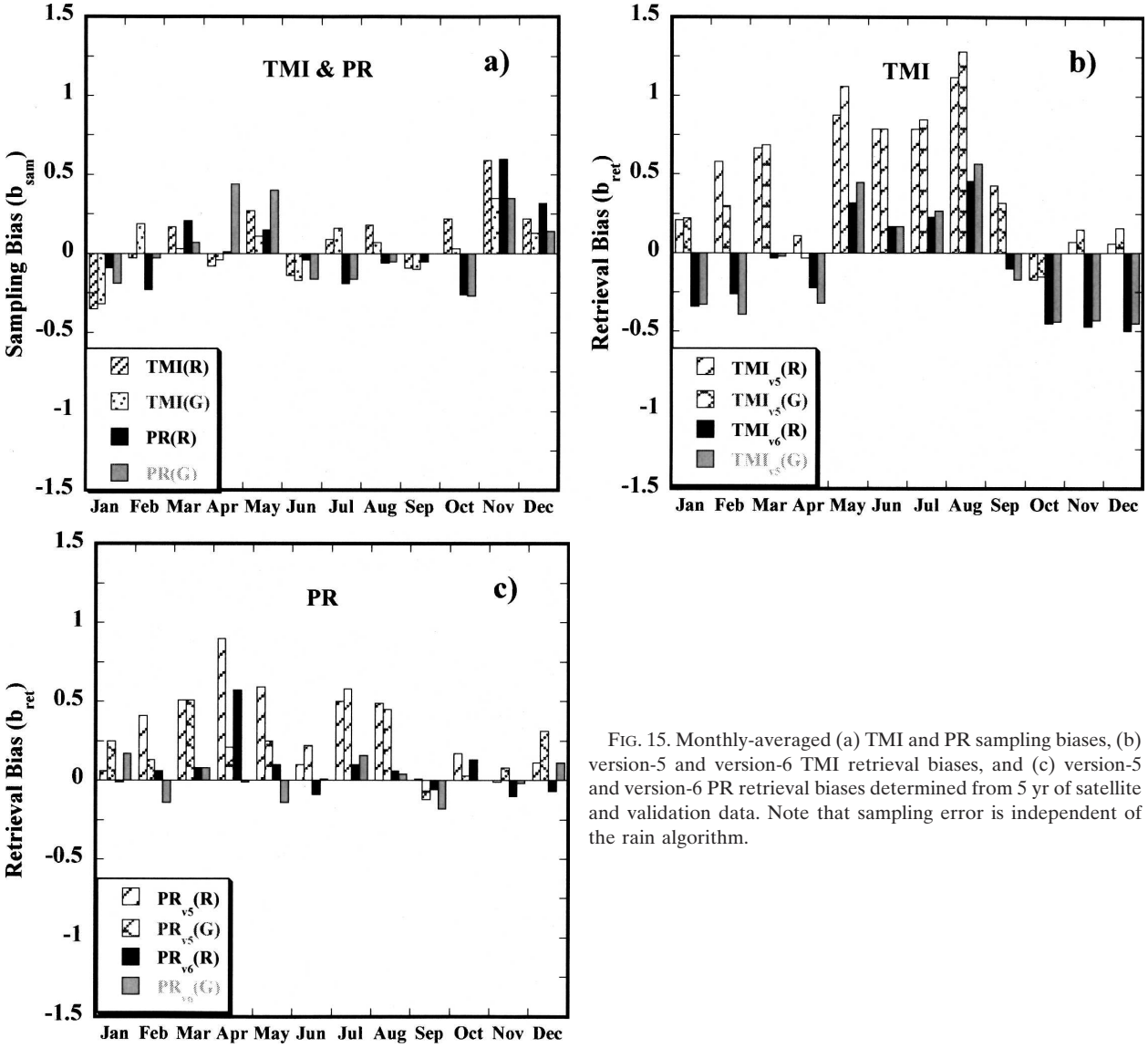

FIG. 15. Monthly-averaged (a) TMI and PR sampling biases, (b) version-5 and version-6 TMI retrieval biases, and (c) version-5 and version-6 PR retrieval biases determined from 5 yr of satellite and validation data. Note that sampling error is independent of the rain algorithm.

and ground-based (r_0) monthly rain estimates should both be evaluated relative to the true rainfall r_T, an unobservable quantity. One of the key challenges of satellite validation then is how to quantify in a meaningful way the error variance of the satellite estimate $\mathrm{var}(s_0 - r_T)$, where r_T is unknown.

A regional-scale, climatological error model was developed that used high-resolution ground data to decompose the total standard error in satellite-derived monthly rainfall estimates into its sampling and retrieval error components. Two distinct monthly rainfall estimates were produced from the ground-based time series. One estimate was computed from an integration of the time series on monthly time scales, while the other was estimated by subsampling the time series at satellite overpass times and then using the monthly rain statistics to derive a sensor-dependent mean monthly rain rate r_S. In this study, the rain parameter r_S performed a critical role in the decomposition of the total error variance, because it was assumed to contain the temporal sampling error of the satellite and so provided an essential connection between sampling and retrievals.

The "true" error variance was approximated as the sum of two uncorrelated variances: $\mathrm{var}(s_0 - r_0)$ and $\mathrm{var}(r_0 - r_T)$. The first expression, characterizing the relative sampling and retrieval errors, was determined by decomposing $\mathrm{var}(s_0 - r_0)$ using r_S. This calculation involved empirical quantities that were readily available. The second expression characterized the absolute

random error associated with the validation sensor but involved r_T, which was unknown. Although this statistical quantity could not be directly estimated, we attempted to establish an upper bound on $\mathrm{var}(r_0 - r_T)$ by applying the error variance separation method.

This climatological error model was applied to 5 yr of satellite and GV rainfall estimates for a gridded region in central Florida. Linear regressions between satellite and subsampled ground-based monthly rainfall estimates resulted in high correlations (>0.9), considerably higher than what is typically observed in most cases for r_0. It is therefore contended based on this result that r_S is more suitable for directly probing satellite retrievals on climatological scales.

Error estimates determined from gridded radar and gauge data were generally in good agreement, suggesting that random radar–gauge errors were effectively minimized at monthly scales. The ratio of PR to TMI random sampling errors closely approximated the theoretical expected sampling error ratio of 1.3, whereas TMI retrieval errors exceeded the retrieval errors for the PR by about a factor of 2. Moreover, it was clearly shown in the case of both rain sensors that the version-6 algorithms reduced the retrieval errors observed in version 5, especially in the case of the TMI. Additional climatological analysis of the annual cycle also found evidence of an alternating seasonal bias in the $\mathrm{TMI}_{\mathrm{v6}}$ rain estimates. In the future, this method will need to be applied over a broader geographical domain so that the error structure in TRMM rainfall estimates can be studied as a function of latitude and climate regime.

Acknowledgments. I thank the two reviewers of this paper for their insightful comments, which led to a constructive revision of the original manuscript. I also thank my wife Houra for dedicating time to assisting me with the technical editing of the manuscript.

REFERENCES

Bell, T. L., and P. K. Kundu, 2000: Dependence of satellite sampling error on monthly averaged rain rates: Comparison of simple models and recent studies. *J. Climate,* **13,** 449–462.

——, and ——, 2003: Comparing satellite rainfall estimates with rain-gauge data: Optimal strategies suggested by a spectral model. *J. Geophys. Res.,* **108,** 4121–4138.

——, A. Abdullah, R. L. Martin, and G. North, 1990: Sampling errors for satellite-derived tropical rainfall: Monte Carlo study using a space–time stochastic model. *J. Geophys. Res.,* **95,** 2195–2205.

——, P. K. Kundu, and C. D. Kummerow, 2001: Sampling errors of SSM/I and TRMM rainfall averages: Comparison with error estimates from surface data and a simple model. *J. Appl. Meteor.,* **40,** 938–954.

Ciach, J. G., and W. F. Krajewski, 1999: On the estimation of radar rainfall error variance. *Adv. Water Resour.,* **22,** 585–595.

Fisher, B. L., 2004: Climatological validation of TRMM TMI and PR monthly rain products over Oklahoma. *J. Appl. Meteor.,* **43,** 519–535.

Gebremichael, M., and W. F. Krajewski, 2004: Assessment of statistical characteristics of small-scale rainfall variability from radar: Analysis of TRMM ground validation datasets. *J. Appl. Meteor.,* **43,** 1180–1199.

Groisman, P. Ya., and D. R. Legates, 1994: The accuracy of United States precipitation data. *Bull. Amer. Meteor. Soc.,* **75,** 215–227.

Habib, E., and W. F. Krajewski, 2002: Uncertainty analysis of the TRMM ground-validation radar-rainfall products: Application to the TEFLUN-B field campaign. *J. Appl. Meteor.,* **41,** 558–572.

Iguchi, T., T. Kozu, R. Meneghini, J. Awaka, and K. Okamoto, 2000: Rain-profiling algorithm for the TRMM precipitation radar. *J. Appl. Meteor.,* **39,** 2038–2052.

Kummerow, C., W. S. Olson, and L. Giglio, 1996: A simplified scheme for obtaining precipitation and vertical hydrometer profiles from passive microwave sensors. *IEEE Trans. Geosci. Remote Sens.,* **34,** 1213–1232.

——, W. Barnes, T. Kozu, J. Shiue, and J. Simpson, 1998: The Tropical Rainfall Measuring Mission (TRMM) sensor package. *J. Atmos. Oceanic Technol.,* **15,** 809–817.

——, and Coauthors, 2000: The status of the Tropical Rainfall Measuring Mission (TRMM) after two years in orbit. *J. Appl. Meteor.,* **39,** 1965–1982.

——, and Coauthors, 2001: The evolution of the Goddard profiling algorithm (GPROF) for rainfall estimation from passive microwave sensors. *J. Appl. Meteor.,* **40,** 1801–1820.

Laughlin, C. R., 1981: On the effect of temporal sampling on the observation of mean rainfall. *Precipitation Measurements from Space: Workshop Report.* D. Atlas and O. Thiele, Eds., NASA, D59–D66.

McCollum, J. R., W. F. Krajewski, R. R. Ferraro, and M. B. Ba, 2002: Evaluation of biases of satellite rainfall estimation algorithms over the continental United States. *J. Appl. Meteor.,* **41,** 1065–1080.

McConnell, A., and G. North, 1987: Sampling errors in satellite estimates of tropical rain. *J. Geophys. Res.,* **92,** 9567–9570.

Meneghini, R., T. Iguchi, T. Kozu, L. Liao, K. Okamoto, J. A. Jones, and J. Kwiatkowski, 2000: Use of the surface reference technique for path attenuation estimates from the TRMM precipitation radar. *J. Appl. Meteor.,* **39,** 2053–2070.

Morrissey, M. L., and J. E. Janowiak, 1996: Sampling-induced conditional biases in satellite climate-scale rainfall estimates. *J. Appl. Meteor.,* **35,** 541–548.

——, J. A. Maliekal, J. S. Greene, and J. Wang, 1995: The uncertainty of simple spatial averages using rain gauge networks. *Water Resour. Res.,* **31,** 2011–2017.

Negri, A. J., T. L. Bell, and L. Xu, 2002: Sampling of the diurnal cycle of precipitation using TRMM. *J. Atmos. Oceanic Technol.,* **19,** 1333–1344.

North, G. R., 1992: Characteristics of tropical precipitation important for estimation by satellites. *The Global Role of Tropical Rainfall,* J. S. Theon et al., Eds., A. Deepak, 169–181.

——, and S. Nakamoto, 1989: Formalism for comparing rain estimation designs. *J. Atmos. Oceanic Technol.,* **6,** 985–992.

Oki, R., and A. Sumi, 1994: Sampling simulation of TRMM rainfall estimation using radar–AMeDAS composites. *J. Appl. Meteor.,* **33,** 1597–1608.

Rosenfeld, D., D. B. Wolff, and E. Amitai, 1994: The window probability matching method for rainfall measurement with radar. *J. Appl. Meteor.,* **33,** 682–693.

Salby, M. L., and P. Callaghan, 1997: Sampling error in climate properties derived from satellite measurements: Consequences of undersampled diurnal variability. *J. Climate,* **10,** 18–36.

Shepard, J. M., B. S. Ferrier, and P. S. Ray, 2001: Rainfall morphology in Florida convergence zones: A numerical study. *Mon. Wea. Rev.,* **129,** 177–197.

Shin, K., and G. R. North, 1988: Sampling error study for rainfall estimate by satellite using a stochastic model. *J. Appl. Meteor.,* **27,** 1218–1231.

Simpson, J., R. F. Adler, and G. R. North, 1988: A proposed Tropical Rainfall Measuring Mission (TRMM) satellite. *Bull. Amer. Meteor. Soc.,* **69,** 278–294.

Spencer, R.W., H. M. Goodman, and R. E. Hood, 1989: Precipitation retrieval over land and ocean with the SSM/I: Identification and characteristics of the scattering signal. *J. Atmos. Oceanic Technol.,* **6,** 254–273.

Steiner, M., 1996: Uncertainty of estimates of monthly areal rainfall for temporally sparse remote observations. *Water Resour. Res.,* **32,** 373–388.

——, T. L. Bell, Y. Zhang, and E. F. Wood, 2003: Comparison of two methods for estimating the sampling-related uncertainty of satellite rainfall averages based on a large radar dataset. *J. Climate,* **16,** 3759–3778.

Thiele, O., 1988: Validating space observations of rainfall. *Tropical Rainfall Measurements,* J. S. Theon and N. Fugono, Eds., A. Deepak, 415–423.

Wilheit, T. T., 1988: Error analysis for the Tropical Rainfall Measuring Mission (TRMM). *Tropical Rainfall Measurements,* J. S. Theon and N. Fugono, Eds., A. Deepak, 377–385.

Williams, S., K. Caeser, and K. Southwick, 1992: Convection and Precipitation Experiment operations summary and data inventory. Office of Field Project Support, Boulder, CO, 425 pp.

Wilson, J. W., and E. A. Brandeis, 1979: A radar measurement of rainfall—A summary. *Bull. Amer. Meteor. Soc.,* **60,** 1048–1058.

Wolff, D. B., D. A. Marks, E. Amitai, D. S. Silberstein, B. L. Fisher, A. Tokay, J. Wang, and J. L. Pippitt, 2005: Ground validation for the Tropical Rainfall Measuring Mission (TRMM). *J. Atmos. Oceanic Technol.,* **22,** 365–380.

Zawadzki, I. I., 1975: On radar-raingage comparison. *J. Appl. Meteor.,* **14,** 1430–1436.